Contrib Mineral Petrol
DOI 10.1007/s00410-011-0660-1

ORIGINAL PAPER

Quartz zoning and the pre-eruptive evolution of the ~340-ka Whakamaru magma systems, New Zealand

N. E. Matthews · D. M. Pyle · V. C. Smith · C. J. N. Wilson · C. Huber · V. van Hinsberg

Received: 6 October 2010 / Accepted: 26 May 2011

Abstract Cathodoluminescence (CL) zoning in quartz crystals from rhyolitic pumices in two ignimbrite members of the ~340-ka Whakamaru super-eruption deposits, Taupo Volcanic Zone, New Zealand, is investigated in conjunction with the analysis of Ti concentration in quartz to reconstruct the history of changing magma chamber conditions and to elucidate the eruption-triggering processes. CL intensity images are taken as a proxy for Ti concentration and thus temperature and/or pressure and/or compositional variations during crystal growth history. Estimates of the maximum temperature changes (i.e., assuming other factors influencing Ti uptake remain constant) are made using the TitaniQ geothermometer based on the Ti concentration in quartz. These results are reviewed in comparison with Fe–Ti oxide, feldspar-melt and amphibole geothermometry. Core-to-rim quartz Ti profiles record a marked change in conditions (temperature increase and/or pressure decrease and/or change in melt composition) causing and then following a significant resorption horizon in the outer parts of the crystals. Two alternative models that could explain the quartz Ti zonation invoke a temperature increase caused by mafic recharge and/or a pressure decrease due to magma ponding and re-equilibration at shallow crustal levels. Concomitant changes in melt composition and Ti activity may, however, also have strongly influenced Ti uptake into the quartz. Some crystals also show other marked increases in CL brightness internally, but any accompanying magmatic changes did not result in eruption. Diffusion modelling indicates that this significant change in conditions occurred over ~10–85 years prior to caldera-forming eruption. This rapid thermal pulse or pressure change is interpreted as evidence for open-system processes, and appears to record a magma chamber recharge event that rejuvenated the Whakamaru magma system (melt-dominant magma plus crystal mush), and potentially acted as a trigger for processes that led to eruption.

Keywords Quartz · Titanium · Geothermometry · Rhyolite · Whakamaru · Taupo Volcanic Zone

Communicated by J. Blundy.

Electronic supplementary material The online version of this article (doi:10.1007/s00410-011-0660-1) contains supplementary material, which is available to authorized users.

N. E. Matthews (✉) · D. M. Pyle · V. van Hinsberg
Department of Earth Sciences, University of Oxford, South Parks Road, Oxford OX1 3AN, UK
e-mail: naomi.matthews@earth.ox.ac.uk

V. C. Smith
Research Laboratory for Archaeology and the History of Art, University of Oxford, South Parks Road, Oxford OX1 3QY, UK

C. J. N. Wilson
School of Geography, Environment and Earth Sciences, Victoria University, PO Box 600, Wellington 6040, New Zealand

C. Huber
School of Earth and Atmospheric Sciences, Georgia Institute of Technology, 311 Ferst Drive, Atlanta, GA 30332, USA

Introduction

The chemical zonation of crystals in igneous rocks provides an important archive of information that may be used in the reconstruction of magma reservoir processes. Detailed petrographic and geochemical analysis of such

Published online: 21 June 2011

zoning can provide constraints on complex thermal and pressure histories and changes in host melt composition or physical parameters of the magma reservoir during crystal growth (e.g., Wallace et al. 1999; Anderson et al. 2000; Humphreys et al. 2006; Liu et al. 2006; Smith et al. 2009). In particular, in silicic systems, trace element concentrations in quartz and their related cathodoluminescence (CL) emission properties provide valuable petrological clues to crystallization conditions (Götze et al. 2004; Wark and Watson 2006).

CL imaging reveals complex zoning in magmatic quartz crystals (e.g., Peppard et al. 2001; Liu et al. 2006; Wark and Watson 2006; Shane et al. 2008a; Smith et al. 2010). Variations in quartz CL intensity are interpreted empirically as relating directly to Ti content, reflecting changes in melt chemistry and/or temperature/pressure during crystallization (Wark and Watson 2006; Thomas et al. 2010). Complex histories are thus indicated by the wide variety of quartz CL-zoning patterns observed, indicating detailed temperature/pressure/composition records present in single pumice clasts. However complex, such histories are central to reconstructing the assembly of the erupted magma body.

Here, we present new geochemical data on the trace element zonation and CL properties of quartz from pumices extracted from specific members of the large-volume (>1,500 km^3) Whakamaru group of ignimbrites from Taupo Volcanic Zone (TVZ), New Zealand (Froggatt et al. 1986; Wilson et al. 1986; Pillans et al. 1996; Brown et al. 1998). The ignimbrites extend over ~13,000 km^2 of central North Island (Fig. 1) and have been previously characterized by field, petrological and geochemical investigations (Ewart 1965; Martin 1965; Briggs 1976; Wilson et al. 1986; Brown et al. 1998; Brown and Fletcher 1999). The deposits comprise five crystal-rich (~15–40% crystal content) ignimbrite units named Whakamaru, Manunui, Rangitaiki, Te Whaiti and Paeroa Range Group ignimbrites (Fig. 1). These units share similar geochemistry and petrography, and each contains varying amounts of five distinct pumice (magma) types (classified as types *A*, *B*, *C*, *D* and *mixed basaltic pumices*) associated with different compositions and crystal contents (Brown et al. 1998). Collectively, these features suggest the magmas underwent complex crystallization processes in multiple chambers. This inference is supported by field evidence for multiple eruptions over a short, but uncertain, time period (Brown et al. 1998; Wilson et al. 1986). Brown et al. (1998) provided evidence that the less-evolved, low-silica rhyolites represent magmas that underwent significant fractionation at shallow crustal levels to produce the dominant volumes of more evolved rhyolites ultimately erupted.

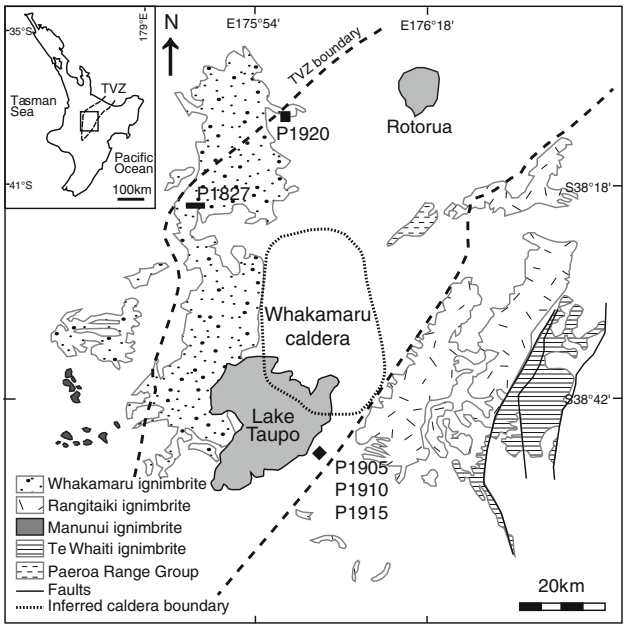

Fig. 1 Sketch map showing location of Whakamaru caldera and the distribution of Whakamaru group ignimbrites, central TVZ (after Brown et al. 1998). Sample localities are marked by *dark grey symbols*: Rangitaiki samples are P1905, P1910 and P1915 (collected from Hinemaiaia B Dam); Whakamaru samples are P1920 (from Sutton Road) and P1827 (Type *D* pumice collected from Edsel Road). Inset map shows North Island of New Zealand and location of TVZ

Here, we investigate the magmatic conditions leading to these caldera-forming eruptions, and the complexity of underlying magma chamber processes, and use diffusion modelling to quantify timescales of significant magma recharge events.

Regional geology

The central TVZ (Fig. 1) is an actively rifting arc segment that has produced rhyolite eruptions at millennial frequency during the late Quaternary (Wilson et al. 1995, 2009), making it a fruitful area for studying processes governing the large-scale production, storage and eruption of rhyolite magma. Mesozoic basement greywackes crop out east and west of the TVZ and underlie the volcanic fill within the zone, either as rifted blocks with intrusions or as tectonically stretched crust (Stern et al. 2006). The very high heat flux (800 mW m^{-2} in the central, rhyolite-dominated portion of the TVZ: Bibby et al. 1995; Hochstein 1995; Stern 1987) causes the brittle-to-ductile transition to occur at 6–7 km depth (Bryan et al. 1999), while seismic refraction data indicate that the quartzo-feldspathic upper crust extends to only 15–16 km depth (Harrison and White 2004; Stratford and Stern 2004). Low *P*-wave velocities (6.9–7.3 km s^{-1}; Stratford and Stern

2004) recorded from below 15–16 km may represent mantle with significant amounts of melt or highly intruded mafic crust with ~2% melt (Harrison and White 2004).

Eruptions in the central TVZ are volumetrically skewed heavily towards rhyolite, with lesser amounts of andesite > dacite > basalt as surficial eruptive units (Cole 1990; Wilson et al. 1995). Isotopic data indicate that the silicic melts are generated from highly fractionated primitive basalt which has been contaminated by the metasedimentary crust (<25%; McCulloch et al. 1994; Graham et al. 1995), although evidence for silicic magma components derived from direct crustal melting is also recorded (Charlier et al. 2008, 2010). The large volumes of mafic magma required to generate the rhyolites, whether by fractionation or crustal melting, are almost entirely trapped within or immediately below the quartzo-feldspathic crust. A characteristic feature of the central TVZ is, however, that mafic melts do reach and interact with the melt-dominant magma bodies at shallow depths (4–8 km) and are not entirely confined within a deeper mush zone (cf. Hildreth 1981, 2004). Mafic magma evidently interacted with the melt-dominant body for the Rangitaiki ignimbrite member of the Whakamaru group (Brown et al. 1998; this paper), for example, as well as in younger eruptions of the Taupo and Okataina volcanoes (e.g., Blake et al. 1992; Wilson et al. 2006; Shane et al. 2008b).

Samples and methods

Here, we apply measurements of Ti concentrations together with interpretations of CL images (Watt et al. 1997; Götze et al. 2001, 2004; Peppard et al. 2001) to studies of Ti zonation in quartz crystals extracted from five pumices sampled from the two most widespread and pumice-rich Whakamaru group ignimbrites, Rangitaiki and Whakamaru (Fig. 1).

We use pumice fragments rather than bulk ignimbrite (cf. Saunders et al. 2010) as these are considered to represent quenched fragments of the vesiculated rhyolite magma, with variations in glass composition between pumices reflecting variations within the parent magma reservoir(s) (Hildreth 1981). Pumices from non-welded parts of the Whakamaru and Rangitaiki ignimbrites were sampled extensively (140 samples) and characterized by whole-rock XRF (Table 1), matrix glass and mineral chemistry (electron microprobe analysis; EPMA) and Fe–Ti oxide compositional data (Table 2). The full data set is provided in the Electronic Supplementary Data. Our sample database was supplemented by 120 pumices previously collected and analysed by Brown et al. (1998).

Table 1 Summary of single pumice samples used in this paper

Pumice sample	Ignimbrite unit	Pumice type	Pumice mineralogy	% crystals	SiO_2 (wt. %)	Rb/Sr	Ti (av. ppm)	FM	T (°C)	Ti (ppm) rutile-saturated melt	a_{TiO_2} (from melt FM)	a_{TiO_2} (from oxides)
P1905	Rangitaiki	*A*	Feldspar,qtz ≫ hbl, opx > biotite ≫ mag, ilm	~25	70.4	0.42	800 (n = 11)	1.74	763	1116	0.72	0.53
P1910	Rangitaiki	*A*	Feldspar, qtz > opx ≫ mag, ilm	~15	70.4	0.65	827 (n = 26)	1.59	768	1125	0.74	0.62
P1915	Rangitaiki	Mixed	Feldspar, qtz > opx, hbl ≫ oliv, mag, ilm (mafic clots)	~25	67.6	0.51	821 (n = 32)	2.01	763	1195	0.69	0.65
P1920	Whakamaru	*A*	Feldspar, qtz ≫ opx ≫ mag, ilm	~20	71.3	0.76	790 (n = 43)	1.55	789	1403	0.54	0.67
P1827	Whakamaru	*D*	Feldspar, qtz ≫ biotite ≫ mag, ilm	~20	72.9	1.83	610 (n = 23)	1.42	740	**1,210 ± 133**	**Av. = 0.67 ± 0.09**	**Av. = 0.66 ± 0.09**

Pumice type is based on Brown et al. (1998) classification scheme. SiO_2 and TiO_2 values are from whole-rock XRF analysis. FM is the melt composition parameter (calculated from Hayden and Watson 2007). For a given temperature, TiO_2 solubility increases as FM increases, or as the melt becomes more mafic; and for a given melt composition as represented by FM, TiO_2 solubility increases with temperature (Hayden and Watson 2007). The single temperature used to calculate rutile saturation and a_{TiO_2} is derived from average Fe–Ti oxide temperatures (using Ghiorso and Evans 2008). The a_{TiO_2} values in the final column are derived directly from oxide compositions. Entries in bold refer to the average values across all pumice samples

Table 2 Geothermometry data (in °C) recorded by Whakamaru crystals

Pumice Sample	Fe–Ti oxides (Ghiorso and Evans 2008)					TitaniQ (Wark and Watson 2006)		Plag-melt equilibria (Putirka 2008)	
	T (°C)	±	logfO_2 NNO	±	n	min	Max	Min	Max
P1905	763	59	+0.41	0.25	20	689	836	763	854
P1910	768	84	+0.30	0.21	26	673	802	788	860
P1915	763	48	+0.39	0.18	21	673	836	757	852
P1920	790	8	+0.35	0.18	66	673	836	785	848
P1827						655	778	730	884

Fe–Ti oxide data for equilibrium pairs; Oxygen fugacity is quoted in logfO_2 relative to NNO buffer, values represent averages from number (n) of Fe–Ti oxide pairs (in equilibrium according to the Bacon and Hirschmann 1988 method), and ± indicates 1 standard deviation. No data from Fe–Ti oxide equilibrium pairs collected for sample P1827. TitaniQ values calculated using an a_{TiO_2} of 0.7. Plag-melt equilibria calculated using only plagioclase feldspar rim data and co-existing glass (by EPMA)

Five pumice samples (Fig. 1; Table 1) were selected for detailed quartz CL study on the basis of mineralogy, clast size, lack of alteration and major-element geochemistry. Type *A* pumice is our main focus as it represents the volumetrically dominant magma type (>95%). Type *D* is also of interest because it may represent a co-erupted but separate chamber with its contrasting isotopic and trace element characteristics (Brown et al. 1998). Types *B* and *C*, in contrast, are likely to represent only second-order variants produced by convective fractionation in a dominantly Type *A* magma reservoir (Brown et al. 1998).

Quartz crystals were extracted by lightly crushing, sieving and hand picking. Approximately, 40 quartz crystals from each pumice sample were extracted, of which 92 were analysed. Crystals are commonly embayed and/or fractured, and thus, only fragments could usually be retrieved. Individual fragments were chosen such that the glass selvedges were still intact on one face. These were mounted in epoxy resin, polished and carbon coated for imaging and analysis. CL images were obtained using a CL detector mounted on a JEOL electron microprobe at the University of Bristol, 15 kV and 22 nA beam current, with image resolution of 1,020 × 790 pixels.

Ti in quartz

Ti concentrations were measured using the JEOL 8600 electron probe in the Research Laboratory for Archaeology and the History of Art, University of Oxford, with a high-beam current (100 nA), extended count times (800 s on peak and background) and 10 μm beam diameter. In order to obtain reliable Ti results at low abundance, Ti was analysed on two spectrometers simultaneously. Merging Ti counts resulted in low detection limits (<10 ppm) and low uncertainties (±11 ppm; 1sd) for Ti. Analysis transects were chosen on the basis of CL zoning, in particular targeting the core–rim interface. Analyses (n = 157) were spaced at 100-μm (av.) intervals (spacing ranged from 45 to 200 μm depending on crystal size) along core-to-rim profiles.

The Ti content of hydrothermally grown quartz is known to be a function of both temperature and pressure, with a ±100 MPa pressure change corresponding to ±20°C change in temperature and vice versa (Thomas et al. 2010). Ti content of quartz (Ti_{qtz}) was proposed (Wark and Watson 2006) to be related primarily to temperature and Ti activity (a_{TiO_2}) of the melt, by Eq. 1 (the "TitaniQ" relationship), where T = temperature (K):

$$T = \frac{-3765}{\log(Ti_{qtz}/a_{TiO_2}) - 5.69} \quad (1)$$

The proposed pressure dependency (Thomas et al. 2010) of Ti in quartz is described by Eq. 2 (output converted to MPa here), where a = 60,952 ± 3,177, b = 1.52 ± 0.39, c = 1,741 ± 63, R is the universal gas constant (8.3145 J K^{-1}), T is temperature (K) and $XQtz_{TiO_2}$ is the mole fraction of TiO_2 in quartz:

$$P(\text{kbar}) = \frac{(-a + bT + RT\ln a_{TiO_2} - RT\ln XQtz_{TiO_2})}{c} \quad (2)$$

Parameters a, b and c have been established by least-squares fitting of experimental Ti-in-quartz solubilities (Thomas et al. 2010). As we note below and discussed by Wilson et al. (2011), the application of this P and T dependency of Ti solubilities leads to implausible results, especially with regard to pressure. Ti partitioning may also be affected by compositional changes in the chamber, affecting the solubility of Ti in the melt.

Constraining Ti activity

None of the Whakamaru group pumices contain rutile, so a_{TiO_2} was estimated as

$$a_{\mathrm{TiO_2}} = \frac{\mathrm{Ti_{melt}}}{\mathrm{Ti_{rut-melt}}} \quad (3)$$

where $\mathrm{Ti_{melt}}$ and $\mathrm{Ti_{rut\text{-}melt}}$ are Ti measured in melt (matrix glass) and rutile-saturated melt (ppm), respectively. $\mathrm{Ti_{rut\text{-}melt}}$ was determined using Eqs. 4 and 5 (Hayden et al. 2005; Hayden and Watson 2007; Table 1):

$$\log(\mathrm{Ti_{rut-melt}}) = 7.95 - \frac{5305}{T} + (0.124 \times \mathrm{FM}) \quad (4)$$

$$\mathrm{FM} = \frac{\mathrm{Na} + \mathrm{K} + 2(\mathrm{Ca} + \mathrm{Mg} + \mathrm{Fe})}{\mathrm{Al} \times \mathrm{Si}} \quad (5)$$

Temperatures and oxygen fugacities (fO_2) were estimated using the Fe–Ti oxide geothermometer (Ghiorso and Evans 2008) with our Fe–Ti oxide data and values from Brown et al. (1998). Only magnetite–ilmenite pairs in Mg–Mn equilibrium, assessed using the Bacon and Hirschmann (1988) method, were used. These calculations indicate that rutile should saturate at Ti concentrations of 1,210 ± 133 ppm (Table 1) and indicate $a_{\mathrm{TiO_2}} = 0.67 \pm 0.09$ (1 sd, range 0.54–0.74). Results are consistent with Oruanui rhyolite (0.74 ± 0.07; Wilson et al. 2011), Bishop Tuff (0.63 ± 0.03; Wark et al. 2007; and 0.53 ± 0.02 to 0.51 ± 0.10; Reid et al. 2010) and the range for large silicic systems of $0.5 < a_{\mathrm{TiO_2}} < 0.6$ (Hayden and Watson 2007). We calculate pressures using both average and end-member activity values, 0.54 and 0.74, respectively (Table 3). Problems arise with this methodology as $a_{\mathrm{TiO_2}}$ calculated using Eq. 4 is dependent on temperature. In order to avoid this problem, Eqs. 1 and 4 can be simultaneously fitted, although this requires the knowledge of the Ti content of the melt from which the crystal zone grew. It cannot be determined whether the concentration of the bulk rock is in equilibrium with the cores of the quartz crystals, so this introduces an additional error.

Activity of rutile in the melt can also be constrained from the coexisting oxides (e.g., Reid et al. 2010). Using end-member thermodynamic properties from the 2004 version of the Holland and Powell (1998) data set, and mixing and disorder models for oxides from White et al. (2000, 2002) and Ghiorso and Evans (2008), temperature, oxygen fugacity and a_{TiO2} can be fitted simultaneously from the set of independent reactions

$$2\ \mathrm{FeTiO_3} = \mathrm{Fe_2TiO_4} + \mathrm{TiO_2} \quad (6)$$

$$6\ \mathrm{FeTiO_3} + \mathrm{O_2} = 2\ \mathrm{Fe_3O_4} + 6\ \mathrm{TiO_2} \quad (7)$$

$$6\ \mathrm{Fe_2O_3} = 4\ \mathrm{Fe_3O_4} + \mathrm{O_2} \quad (8)$$

and the activities of the respective end members in the oxide solid solutions (see Supplementary Data 1). The use of a full thermodynamic model including non-ideality in mixing and disorder for the oxides allows for calculations of all equilibria, despite low activities for some of the end members involved. Across all pumice samples, the weighted average $a_{\mathrm{TiO_2}} = 0.66 \pm 0.09$ (1sd; Supplementary Data 1). There are, however, uncertainties with this methodology. If it is accepted that the oxides re-equilibrate on a short timescale to reflect different conditions (e.g., Venezky and Rutherford 1999; Devine et al. 2003), then the oxides do not reflect conditions during quartz crystal growth, except for their outermost portions (if no resorption). Their present composition can therefore only provide information on $a_{\mathrm{TiO_2}}$ for final quartz growth.

The presence of coexisting oxides throughout quartz crystallization indicates that Ti activity was buffered. However, the buffered value of $a_{\mathrm{TiO_2}}$ will vary with changes in melt composition, temperature and pressure. In an attempt to quantify these relative changes in $a_{\mathrm{TiO_2}}$, melt and coexisting oxide compositions were modelled using rhyolite-MELTS (Gualda et al. 2010). Changes in melt composition and $\mathrm{TiO_2}$ content predict an increase in $a_{\mathrm{TiO_2}}$ for our preferred P–T path (increasing T with decreasing P), but oxide compositions predict a decrease. The magnitude of the change for the full range of quartz crystallization conditions of our P–T path is significant and predicted to be of the order of $\Delta a_{\mathrm{TiO_2}} = 0.2$. Nonetheless, this systematic change in $a_{\mathrm{TiO_2}}$ is insufficient to explain the

Table 3 Pressure and temperature estimates for quartz rims and cores using end-member $a_{\mathrm{TiO_2}}$ values

Quartz crystal zone	$a_{\mathrm{TiO_2}}$	Av. pressure (MPa)	1sd	P range (MPa)	Av. temp (°C)	1sd	T range (°C)
RIM	0.5	663	0.81	553–837	849	32	757–886
CORE	0.5	922	1.99	553–1,313	767	38	689–864
RIM	0.7	830	0.81	720–1,004	802	30	717–836
CORE	0.7	1,065	2.37	553–1,480	727	35	655–816
RIM	1	1,008	0.81	898–1,182	756	27	678–787
CORE	1	1,217	2.85	553–16.58	687	32	621–770

Estimates of pressure based on the Thomas et al. (2010) formulations (at fixed temperature of 770°C) and temperature based on equations from Wark and Watson (2006) TitaniQ, using end-member $a_{\mathrm{TiO_2}}$ values from calculations and in comparison with an $a_{\mathrm{TiO_2}}$ of 1 (providing minimum temperature estimates)

differences in Ti concentrations between core and rim and does not modify the trends in temperature that are calculated here from TitaniQ thermometry, although it suggests a smaller temperature range when using the Δa_{TiO_2} from modelled oxide compositions.

These uncertainties in a_{TiO_2} values mean that TitaniQ temperatures must be interpreted as *estimates* only, providing reliable and useful constraints on relative changes. Owing to the contradictory results from our modelling of Δa_{TiO_2} with changing *P–T* conditions, its inclusion in calculating temperatures is unwarranted at present, and calculations in this manuscript, instead, use a fixed a_{TiO_2} of 0.7, with interpretations restricted to relative changes in temperature.

Feldspar-melt and amphibole geothermobarometry

Plagioclase–melt equilibrium temperatures for each sample were calculated using the Putirka (2008) geothermometer, by pairing matrix glass compositions with plagioclase rim data. Values are interpreted with caution, however, as plagioclase–melt equilibria are dependent on dissolved volatile contents (not specifically constrained here) and feldspar rims may not be in equilibrium in the melt when erupted (e.g., Saunders et al. 2010). Amphibole geothermobarometry was applied to the full set of amphibole data from Brown et al. (1998) using the Ridolfi et al. (2010) formulation. These pre-existing data cannot provide the high-resolution thermal history that may be obtained from application of TitaniQ to zoned quartz, but provide a useful overall comparison in terms of the eruptive temperatures and pressures of the host magma.

CL zoning and Ti correlation

Quartz CL brightness is known to correlate with both Ti and Al concentrations (Liu et al. 2006; Wark and Watson 2006; Rusk et al. 2008), suggesting that they are important contributors to CL activity in magmatic quartz. Previous studies have shown that there is a linear relationship between Ti, Al and CL intensity (e.g., Rusk et al. 2008). Thus, greyscale (a numerical value assigned to brightness) values of CL images can be used as a proxy for Ti content, and continuous Ti profiles across all crystal zones can be interpolated from a greyscale calibrated by individual Ti measurements. Correlation between greyscale and EPMA Ti concentrations used in the calibration here was statistically significant (R^2 0.75–0.99), and the greyscale profiles provide a highly resolved record of the Ti uptake during quartz crystallization. The accompanying estimated temperature profiles express changes in Ti concentration purely in terms of temperature and ignore dependencies on pressure and melt composition that must accompany any temperature changes. Whatever the causes, the core-to-rim traverses clearly provide a detailed record of changes (temperature/pressure/composition perturbations) throughout crystal growth.

Results

Pumice petrography

The pumice samples studied here are characterized by a mineral assemblage of plagioclase, quartz ≫ hornblende, orthopyroxene > biotite ≫ magnetite, ilmenite and zircon (Table 1). Total phenocryst contents in the selected pumices range from ~15 to 25%. Fe–Ti oxides are present both as free crystals and hosted within orthopyroxene phenocrysts. Some Rangitaiki pumice displays petrographic textures that imply contact with, and intermingling of, mafic magma and silicic melt. In addition, basaltic andesite and andesitic enclaves are common, containing sieved or strongly oscillatory-zoned plagioclase and aggregates of pyroxene, and crystal clots of amphibole, respectively (Supplementary Fig. 1). Whakamaru pumice also contains some aggregates of strongly zoned plagioclase phenocrysts (An_{25} to An_{43}) and a ferromagnesian assemblage dominated by biotite rather than amphibole.

Glass compositions

Matrix glass fragments derived from Whakamaru group pumices range from 74.9 to 78.9 wt% SiO_2, 0.30–1.00 wt% CaO, 4.46–6.83 wt% K_2O, 2.03–3.39 wt% Na_2O and 0.18–1.58 FeO^T (n=97; anhydrous; see Supplementary Data 2). Glass TiO_2 ranges from 0.08 to 0.22 wt%, and this limited variability is likely to have little influence on the assumption of near-fixed a_{TiO_2}. Whole-rock geochemistry of the mafic inclusions in mingled Whakamaru pumices is characterized by 51.7–53.4 wt% SiO_2, 8.06–9.76 wt% CaO, 0.62–0.78 wt% K_2O and 2.04–2.84 wt% Na_2O (Supplementary Data 3).

Quartz characteristics

Quartz comprises 20–40% of the crystal fraction in Whakamaru and Rangitaiki pumices and characteristically occurs as large, fractured and partially resorbed crystals 0.3–12 mm in diameter (Fig. 2). Quartz crystals are mostly anhedral—assumed to be due to resorption caused by changing conditions prior to eruption. They are also extensively fractured, most likely due to fragmentation caused by melt-inclusion explosion during pre-eruptive overheating and/or decompression, and syn-eruptive shattering (e.g., Tait 1992; Bindeman 2005).

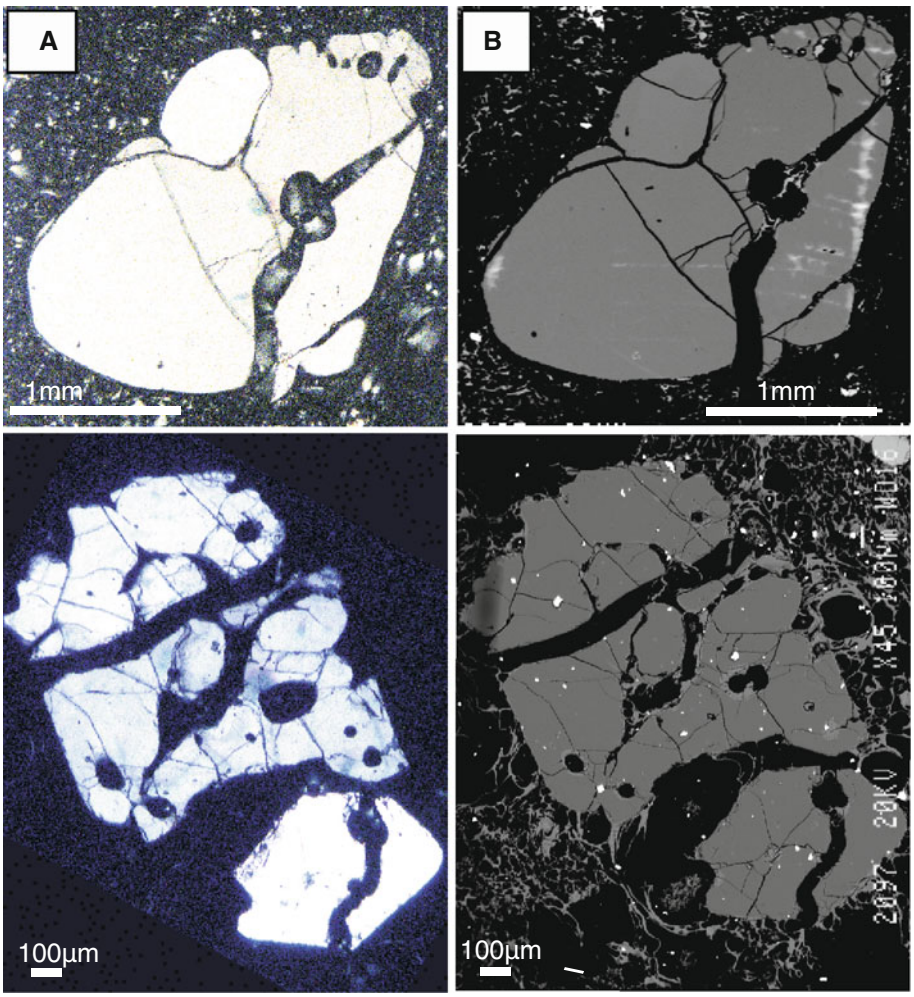

Fig. 2 **a** Optical microscope images of quartz from samples P1905 and P1915; **b** Back-scattered electron (BSE)-SEM images of quartz. Note fractured nature of quartz phenocrysts and resorption boundaries

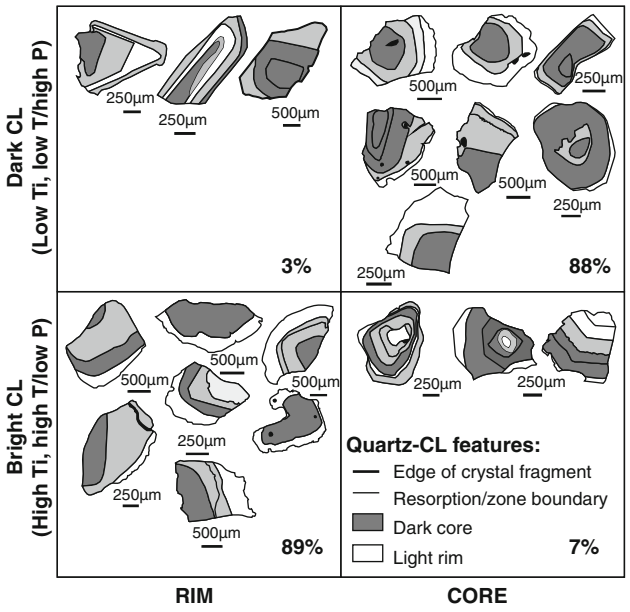

Fig. 3 Summary of quartz CL-zoning patterns. *Bright*-CL rims and *dark* cores are most characteristic of Whakamaru quartz

CL imaging reveals distinct growth zonation, most commonly with a dark-CL cores and bright rims of varying width (Supplementary Fig. 2; Figs. 3, 4). Oscillatory zoning is a characteristic of all quartz grains examined, often truncated by resorption surfaces. The most notable feature is the sharp contrast in CL intensity along the profile, defining a core–rim boundary marked by a dissolution/resorption surface truncating core growth zones (Fig. 4).

Resorbed and embayed parts of crystals and dissolution surfaces are found throughout the crystals but are prominent at the core and near the rim. Resorption surfaces are typically rounded or display complex dissolution patterns and are often associated with a bright-CL zone. These variations in CL correspond to marked increases in Ti (up to 100 ± 10 ppm) occurring over distances of <60 µm (Fig. 4). Rims are Ti rich (bright CL; 90–138 ppm Ti) and are generally narrow (<100 µm). Cores display dark CL (Ti poor: 30–96 ppm) with internal zonation truncated by a resorption surface around which the bright rims have crystallized.

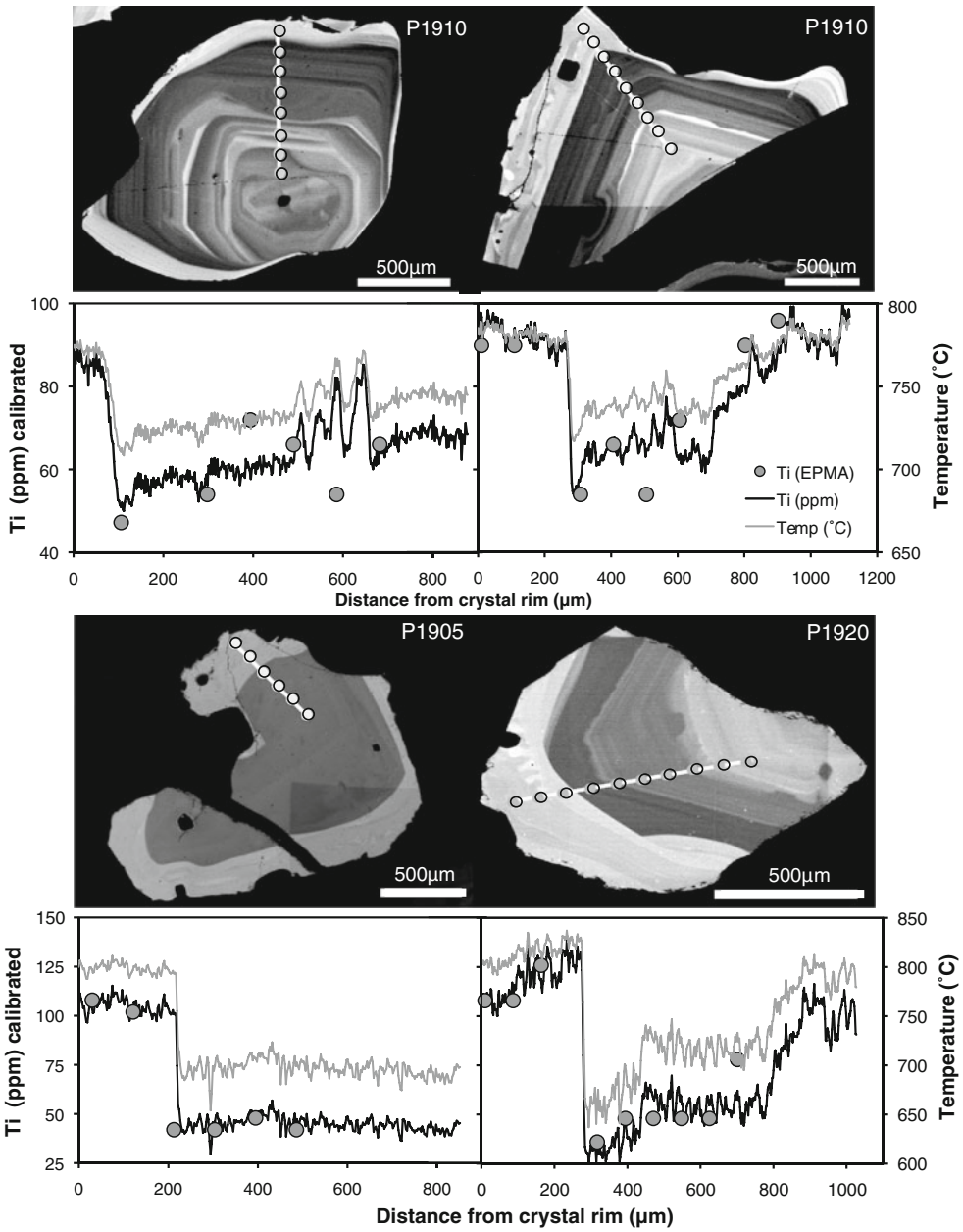

Fig. 4 Selected CL images, showing location of EPMA transects. Profiles from rim to core across quartz crystals show calibrated Ti (*black line*) and temperature (*grey line*). The original EPMA Ti analyses used in the calibration are marked by *grey circles*. The temperatures are estimated from TitaniQ using a single a_{TiO_2} of 0.7 and constant Ti concentrations in the melt

Magmatic temperature estimates

Crystallization temperatures (Table 2; Fig. 5) were estimated by four methods based on Fe–Ti oxides, plagioclase–melt equilibria, amphibole chemistry and TitaniQ (across CL zones in quartz crystals, core to rim). Over all pumice samples, the four suites of temperature estimates range from 647 to 968°C but display a strong mode at 770°C (Fig. 5). Oxygen fugacity was estimated from Fe–Ti oxide equilibria (Ghiorso and Evans 2008), with values for all pumice clasts ranging from −0.03 to 1.08 ± 0.17 (1sd) log units above the nickel/nickel oxide (NNO) buffer (Table 2; Fig. 6).

Plagioclase–melt temperatures calculated using plagioclase rim ($An_{33\pm7}$) and matrix glass (melt) compositions suggest magma temperatures of 817 ± 28°C (1sd) (Fig. 5; Supplementary Data 5). Plagioclase phenocrysts are commonly resorbed, suggesting they were not crystallizing at the time of eruption and therefore do not record eruption temperatures. Amphibole geothermometry using the Ridolfi et al. (2010) formulation provides a comparable temperature range of 745–975°C (error of ±22°C; Supplementary Data 6), with a bimodal trend and strong modes at 770 and 860°C (Fig. 5). The wide temperature range reflects changing temperature conditions recorded during amphibole crystallization. The Fe–Ti oxide temperatures

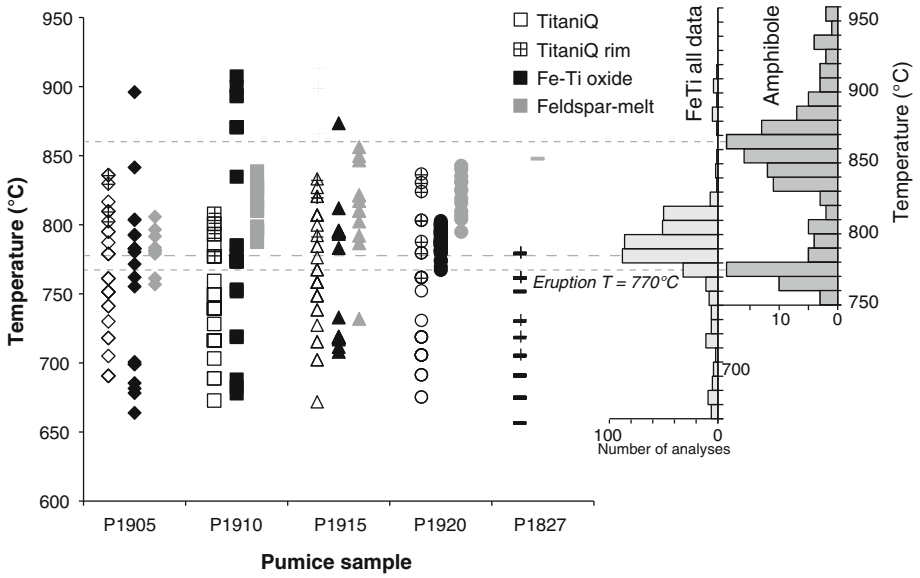

Fig. 5 Comparison of temperatures obtained from TitaniQ, Fe–Ti oxides and feldspar-melt geothermometry for selected single Whakamaru pumice clasts. TitaniQ temperatures calculated from Wark and Watson (2006); Fe–Ti oxide temperatures calculated from Ghiorso and Evans (2008) for magnetite–ilmenite equilibrium pairs (Bacon and Hirschmann 1988); feldspar-melt temperatures from Putirka (2008). The first histogram on the *left* shows Whakamaru Fe–Ti temperatures recalculated from Brown et al. (1998) data for comparison. The second histogram (*right*) displays amphibole temperatures calculated from Brown et al. (1998) data using the Ridolfi et al. (2010) formulation. The *dashed grey lines* show modes for Fe–Ti oxide and amphibole temperatures

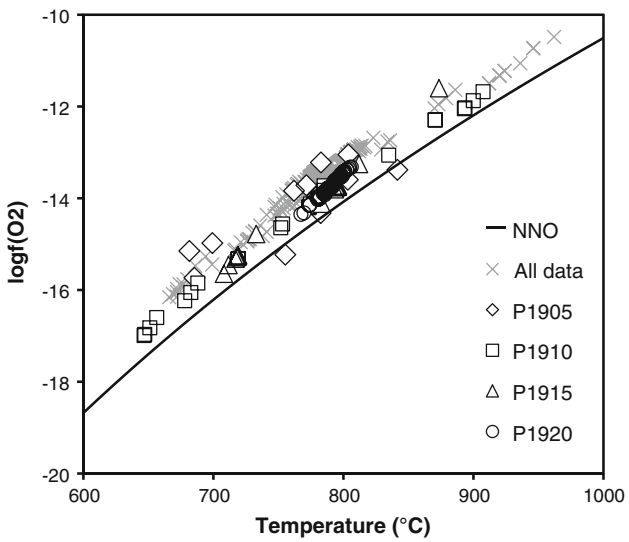

Fig. 6 Temperature and oxygen fugacity calculated for titanomagnetite–ilmenite pairs from Whakamaru pumices, following Ghiorso and Evans (2008). Results for the five Whakamaru pumice clasts and recalculated values from Brown et al. (1998) are plotted. Samples are identified in *inset*. NNO buffer curve after Huebner and Sato (1970) determined at 1 *bar*. Data are provided in the Supplementary Data 4 and 4a

have a strong mode coincident with the amphibole temperatures from the Ridolfi et al. (2010) formulation (Fig. 5).

The use of a single a_{TiO_2} value for all quartz crystal zones is an oversimplification given the interdependence with temperature that is changing concurrently. Ti concentrations in Whakamaru quartz range from 30 to 138 ppm (±11 ppm, 1sd), corresponding to temperatures of 655–836°C (±15°C, 1sd) using TitaniQ (Wark and Watson 2006; Table 3; Fig. 5; Supplementary Data 7) and assuming no pressure dependence (cf. Thomas et al. 2010), constant a_{TiO_2} and no other causes for variations in Ti uptake (cf. Wilson et al. 2011). The lowest values are recorded in the crystal core and typically increase in a fluctuating stepwise pattern towards the rim (Fig. 4). Maximum temperatures recorded from quartz rims are too high for quartz crystallization in a rhyolite melt (Hammer 2008), implying these high temperatures are misleading and likely to be related to either boundary layer kinetics or errors resulting from the assumption of constant a_{TiO_2} and no pressure dependency.

Whakamaru and Rangitaiki TitaniQ values are broadly consistent with Fe–Ti oxide equilibrium temperatures (Fig. 5), although they display a greater temperature range. This is expected since the Ti contents and consequent TitaniQ temperatures are related to individual crystal zones over the growth history of the crystals. This disparity in temperature records can also be attributed to differences in the rates of diffusion in the different mineral phases. Elemental diffusion is faster in Fe–Ti oxides than in quartz. Diffusion of Ti in quartz is given by Eq. 9

$$D_{Ti} = 7 \times 10^{-8} \exp(-273 \pm 12\,\mathrm{kJmol^{-1}}/RT)\mathrm{m^2 s^{-1}}, \quad (9)$$

(parallel to the 001 axis, 700 $< T <$1,150°C; Cherniak et al. 2007), whereas Fe–Ti oxides re-equilibrate by diffusion on timescales of days to months (Devine et al. 2003). Oxide temperatures thus reflect more the temperature of eruption (Devine et al. 2003) rather than thermal fluctuations during crystal growth. The large range in temperature determinations from Fe–Ti oxides observed here (Figs. 5, 6) is potentially due to pluton recycling (with lower estimates being subsolidus). The 770°C mode recorded by the Fe–Ti oxides (and amphibole) is thought to reflect the final reheating temperature on eruption and is not recorded by the quartz rims due to resorption.

Magmatic pressure estimates

The quartz–albite–orthoclase (Qz–Ab–Or) projection of glass major-element analyses from single pumice clasts (Fig. 7; Blundy and Cashman 2001) indicates low closure pressures of 50–150 MPa. In silica- and water-saturated magmas like these, this pressure estimate may represent the final storage pressure at which quartz and feldspar crystallized and the melt composition was 'frozen'. Assuming an average uppermost crustal density of 2,500 kg m^{-3}, these pressures suggest shallow depths (~2–6 km) of crystallization of the major mineral phases for Whakamaru and Rangitaiki magmas prior to eruption.

The Putirka (2005, 2008) feldspar-melt geothermometer provides an average pressure of 235 MPa (1sd; ~9 km depth) and H_2O content of 4.01 ± 0.69 wt%. This is consistent with water contents of 4.3–4.7 wt% in inherited Whakamaru-like melt inclusions in Oruanui quartz cores (Liu et al. 2006). Plagioclase compositions are sensitive to pH_2O, temperature and pressure, however, so the model cannot determine which variables were changing, and it is likely that they were changing simultaneously.

Pressures were also calculated from amphibole compositions using the formulations of Ridolfi et al. (2010) and the full suite of Whakamaru and Rangitaiki samples from Brown et al. (1998). Calculations yield a strong mode of 110 ± 14 MPa (70–409 MPa; Supplementary Data 6), indicating hornblende crystallization at crustal depths of ~5 km.

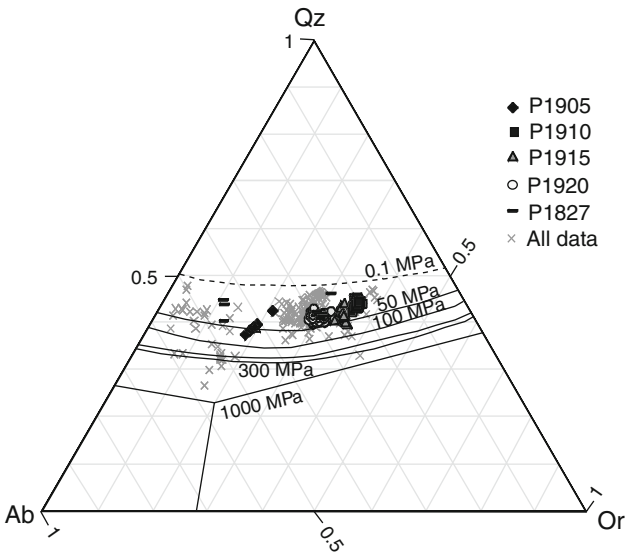

Fig. 7 Major-element glass matrix glass compositions for the Whakamaru pumice samples plotted on the Qz–Ab–Or–H_2O system, following Blundy and Cashman (2001). Closure pressure estimates range from 50 to 150 MPa for the Whakamaru pumices. *All data* refers to data from Brown et al. (1998)

Discussion

Quartz zoning patterns

Contrasting bimodal light/dark-CL zonation is apparent in almost all crystals with 88% showing dark (low-Ti) cores and 89% with light (high-Ti) rims (Fig. 3). The darker cores crystallized at a lower-temperature range (655–787°C by TitaniQ; Wark and Watson 2006), or with higher pressure or melt a_{TiO_2}, whereas rims involved higher-temperature crystallization, 778–836°C (and/or lower-pressure and/or Ti activities in the melt). We note that quartz is unstable at the maximum temperatures calculated by TitaniQ here (Hammer and Rutherford 2002; Hammer 2008), and it is likely that melt composition and the dependence of a_{TiO_2} on temperature play important roles in Ti partitioning. Dark cores are truncated by a resorption horizon, suggesting that changes in melt composition and/or temperature/pressure interrupted crystallization for a period. By analogy with the Bishop Tuff (Wark et al. 2007), this period may have been associated with recharge: represented during eruption by the basaltic andesite enclaves. A minority of crystals display a resorbed light-CL core (7%; Fig. 3), suggesting initial crystallization from higher-temperature (and/or lower pressure/a_{TiO_2}) magma, or reflecting mixing of crystals between different zones in a thermally heterogenous magmatic system. Another minor population of crystals was characterized by anhedral dark-CL crystal rims (3%; Fig. 3).

Interpolated transects across crystals (Fig. 4) suggest that abrupt periodic temperature increases (av. 66°C; max 105°C), assuming uniform pressure and a_{TiO_2}. Conversely, at a constant temperature, these changes would require an unrealistically large pressure decrease (300 MPa, equivalent to ~12 km rise: Thomas et al. 2010) or a sharp a_{TiO_2} decrease of ~0.4. The changes are especially pronounced at inner margins of crystal rims and are characteristic of quartz from the Whakamaru (s.s.) and Rangitaiki

ignimbrites. In Fig. 4, for example, the four crystals show sharply defined Ti increases of 53–67 ppm, equivalent to temperature increases of 80–110°C within 300 μm of the crystal rim, while other samples show smaller pulses in increments of 38–52 ppm Ti, equivalent to 60–90°C closer to the core (300–600 μm from rim). In addition, some crystals show separate sequential temperature spikes of up to 100°C further from the rim (>500 μm). Crystals thus experienced fluctuating conditions throughout crystallization, with the most significant thermal event occurring towards the rim. The smaller Ti spikes may reflect the kinetics of crystal growth and incorporation of high-Ti from boundary layers, which is feasible if growth is more rapid than diffusion. This competition between crystallization and diffusion timescales can be defined by a Damköhler number (Ruprecht et al. 2008), *Da*, as follows

$$Da = \frac{t_{ad}}{t_{react}}, \quad (10)$$

where t_{ad} is the theoretically derived advection timescale (Linden and Redondo 1991) and t_{react} is the crystallization or dissolution timescale. Using estimated quartz growth rates (3×10^{-7} μm s^{-1}, see calculations in diffusion section) as $t_{react,}$ and diffusion at 770°C (1.5×10^{-15} μm^2 s^{-1}) as t_{ad}, we find that Da $\leq$ 1, which implies that crystallization is fast enough to explain the smaller Ti spikes, rather than being diffusion controlled. The compositional boundary which is the focus of diffusion modelling here is a more significant feature, however, and therefore not affected by competition between growth rate and diffusion.

Using the Thomas et al. (2010) model and a fixed pressure of 235 MPa (from feldspar-melt calculations), ranges in quartz rim and core temperatures are 681–753°C (av. 722 ± 25°C; 1sd) and 582–721°C (av. 645 ± 34°C, 1sd), respectively. These are significantly lower than values obtained from TitaniQ. Furthermore, using quartz entrapment pressures recorded from inferred Whakamaru-derived melt inclusions (110–140 MPa; Liu et al. 2006), the temperatures range from 654 to 723°C for quartz rims and 558 to 693°C for cores. These temperatures are below the granite solidus for many pressures equivalent to crustal depths and seem implausible at geologically reasonable pressures for Whakamaru magmas.

Pressure within the system

As described above, new experimental data from Thomas et al. (2010) demonstrated a pressure effect on Ti solubility in hydrothermally grown quartz, with CL zoning being produced solely by pressure changes at constant temperature. Variations in Ti could therefore reflect temperature, pressure, melt composition or a combination of these variables, affecting previous interpretations of TitaniQ results. Application of the Thomas et al. (2010) pressure–Ti relationships provides a broad pressure range of 800–1,150 MPa at a fixed temperature (av. 1,100 ± 200 MPa; $a_{TiO_2} = 0.7$; calculated at average 825°C rim temperature; Table 3). Quartz rims correspond to pressures of 800 ± 100 MPa (1sd), and dark cores, to 1,100 ± 200 MPa (1sd), equivalent to depths of ~32–44 km (assuming crystallization at the same temperature). These pressures would suggest initial crystallization in the mantle below TVZ and are thus neither feasible for quartz crystallization in the TVZ context (e.g., Nairn et al. 2004; Wilson et al. 2006) nor consistent with interpretations of crustal structure (e.g., Harrison and White 2004; Stratford and Stern 2004). As we show below, we consider that crystallization pressures are better constrained by other methods.

Liu et al. (2006) reported partially resorbed dark-CL cores in some of the quartz in pumices from the 27-ka Oruanui deposits (Taupo). The trace element characteristics of melt inclusions in these dark-CL cores followed a pattern distinctly different to the other quartz-hosted melt inclusions, involving a Ba-compatible phase. The close compositional similarity between these anomalous inclusions in dark-CL quartz to those of Whakamaru *type D* pumice (analysis SB1119, from Brown et al. 1998) suggests that these quartz cores represent recycled Whakamaru-age plutonic material (see Charlier et al. 2010). Entrapment pressures from water (4.4 ± 0.1 wt%) and CO_2 (62 ± 20 ppm) contents measured by FTIR of inclusions in the Whakamaru quartz cores are 113–140 MPa (Liu et al. 2006), indicative of quartz growth at depths of 4–5.5 km.

Glass chemistry, feldspar-melt and amphibole geothermometry and quartz melt-inclusion data all suggest that the crystallization of the mineral assemblage dominantly occurred at shallow depths, at pressures of 50–150, 120–650 (Putirka 2008), 110 (mode; Ridolfi et al. 2010) and 110–140 MPa (Liu et al. 2006), respectively. These values suggest that the Thomas et al. (2010) model does not correctly account for the pressure dependence in this system (Wilson et al. 2011). It is likely that the pressure affects Ti solubility in the melt and partitioning into quartz, but its relative effect is not yet adequately quantified. Similarly, the effects of water and other anions in the melt on Ti partitioning have not yet been quantified (e.g., Wilson et al. 2011), and therefore, we cannot assess how the observed Ti changes relate to these parameters.

Diffusion timescales: crystal mush rejuvenation

The majority of the quartz crystals examined in this study show bright rims, as reported for later-erupted Bishop Tuff samples (Wark et al. 2007), implying that they underwent a

significant change in physical and/or chemical conditions not long before eruption as discussed above. The petrographic and chemical evidence for mafic magma involvement during the eruption (particularly the presence of mixed mafic pumices) suggests that this significant change is likely also to have been associated with a recharge event. Any linkage between specific magma recharge events and eruption depends on constraining the time periods involved. The recharge timescale (time elapsed between recharge/quartz rim crystallization and eruption, excluding an unquantifiable period associated with the resorption event) is estimated here using the Ti diffusivities and activation energies from Cherniak et al. (2007), building on the approach of Morgan et al. (2004) and Wark et al. (2007). A 1D diffusion modelling method is considered appropriate because diffusion spans only a small distance across the core–rim boundary. This method relies on measuring the width of Ti zone boundaries in quartz (with the width being dependent on Ti diffusion rate under the ambient conditions), assuming that the major step in Ti content observed in quartz grains was originally sharp but was smeared out over time (Wark et al. 2007). Results provide maximum timescales because the compositional gradient is modelled as being solely due to diffusion, but may also have been influenced by changing melt compositions/temperature/pressure conditions (e.g., Costa and Morgan 2011).

The diffusion rate of Ti in quartz ranges from 1.6×10^{-16} μm^2 s^{-1} at 700°C to 4.9×10^{-14} μm^2 s^{-1} at 900°C (Cherniak et al. 2007). Thermal records are therefore preserved over long periods in quartz crystals in pre-erupted magmas (>10 ka; Cherniak et al. 2007). Once crystal nucleation has occurred, crystallization in a melt is controlled by the relative rates of diffusion of components in the melt and by rates of crystal growth (Watt et al. 1997). Modelling of compositional gradients for the observed CL-zoning patterns thus enables the estimation of crystal residence times in the magmatic system between the event and eruption.

Diffusion times are calculated here at the eruption temperature of 770°C. We use an activation energy of 273 ± 12 kJ/mol, which was experimentally measured for diffusion parallel to the c-axis in synthetic quartz, and a Ti diffusion rate of 2.7×10^{-15} μm^2 s^{-1} (Cherniak et al. 2007). Anisotropy in quartz-hosted Ti diffusion is minor (<5% difference between diffusion rates normal and parallel to quartz *c*-axis), so we do not need to account for the orientation of the crystals used for CL imaging (as a comparison, Ti diffusion normal to the *c*-axis in synthetic quartz is 2.21×10^{-15} μm^2 s^{-1} at 850°C; Cherniak et al. 2007).

Ti gradients along calibrated profiles (Fig. 4) were modelled focusing on boundaries between the large-magnitude Ti increases from dark-CL core to bright-CL rim, occurring over distances of 10–30 μm (Figs. 4, 8; with greyscale resolution of 2 μm). Compositional traverses were taken perpendicular to crystal margins where possible (see Costa et al. 2008), and in 1D modelling, we account trigonometrically for any angle between the zonation and the analysis transect. Best-fit solutions were determined by modelling Ti-compositional profiles for different timescales and choosing the profile that most closely fitted the gradient of the measured greyscale-calibrated Ti profile. The solution to the diffusion of an initial step in concentration is given as

$$C = \frac{1}{2}\mathrm{erfc}\left(\frac{x}{2\sqrt{Dt}}\right), \tag{11}$$

where C is normalized Ti concentration (between 0 and 1), D is width of the boundary, x is position in microns centred on the step, erfc is the complementary error function, and t is the time. In an ideal situation, the measurement of a single concentration and the distance between the measured point and the midpoint (i.e., where $C_m = 0.5$) allow us to calculate the time for Ti diffusion in a quartz crystal using Eq. 12,

$$t = \frac{\Delta x^2}{4D(\mathrm{inverfc}(2C_m))^2} \tag{12}$$

where C_m is the measured normalized concentration and Δx its distance from the midpoint. This approach accounts for the angle (α) between the measured profiles and the Ti concentration gradient by rescaling Δx with $\Delta x \cos(\alpha)$ (derivation in Appendix), thus accounting for artificial lengthening of the profile. The main source of uncertainty in the calculated diffusion times is temperature uncertainty, as diffusion time is exponentially related to temperature (e.g., 1 year of diffusion at 800°C would take 30 year at 700°C and 1,300 year at 600°C). The assumption that this temperature is fixed for diffusion is also an oversimplification, as diffusion would have continued during any thermal fluctuations prior to eruption (Shaw 2004). The temperature error is limited in this study, however, due to reliable constraints from Fe–Ti geothermometry. The assumption that the compositional step was initially vertical introduces an additional unquantifiable error in this simple modelling approach. Nor can 1D modelling account for 2D complexities, so sectioning of the crystal may cause overestimation of timescales (e.g., Martin et al. 2008).

The calculated diffusion timescales are in the year range 10–85 at 770°C (Fig. 8; eruption temperature from Fe–Ti oxides). This timescale is long enough to allow for the growth of the bright rims, without having the recharge event directly linked to triggering of the eruption (cf. Sparks et al. 1977). The width of bright crystal rims is variable, 100–400 μm (minimum width), implying

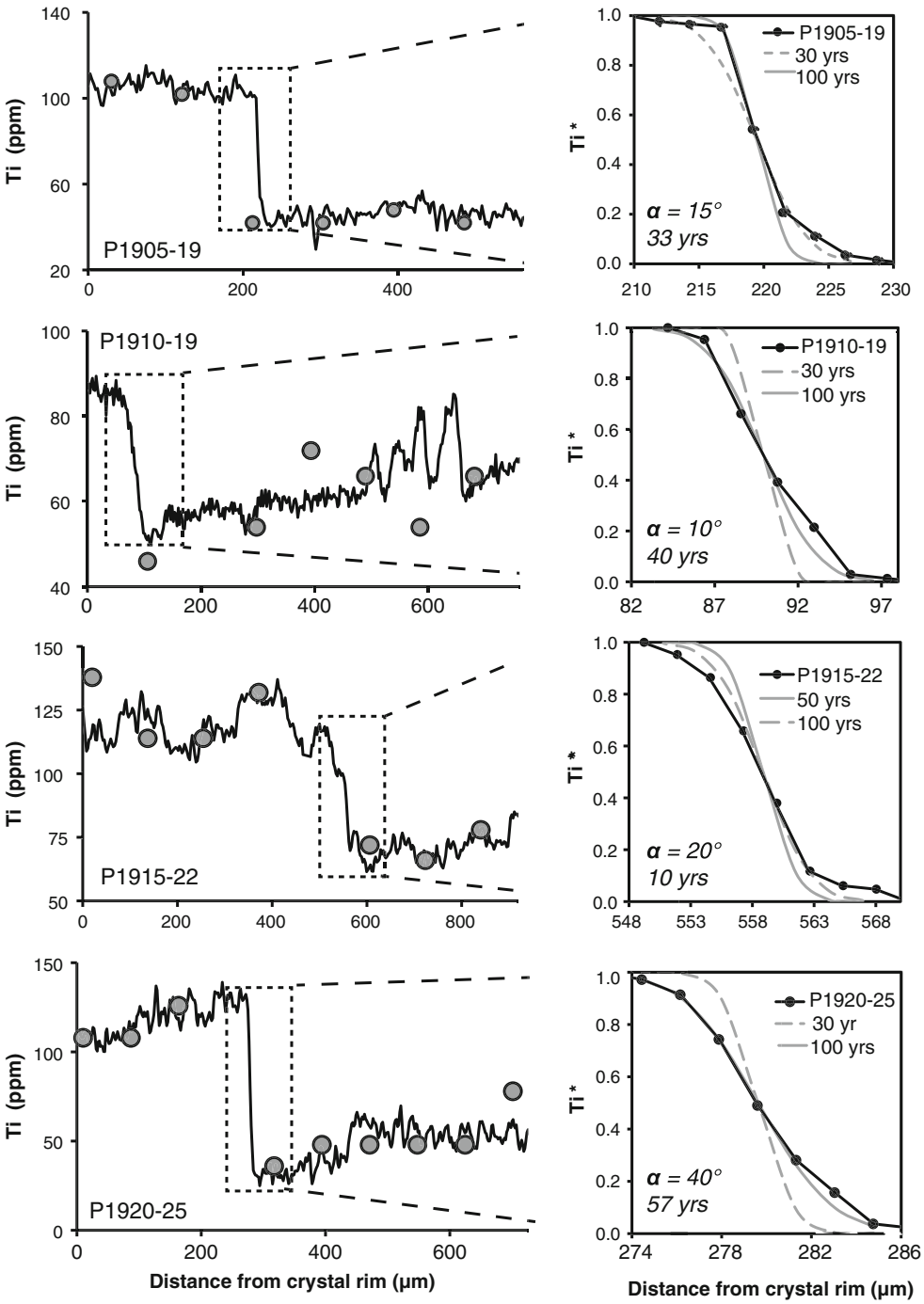

Fig. 8 Diffusion models for Ti in quartz at eruption temperature of 770°C. Graphs (*left*) show CL *greyscale* profiles calibrated to Ti concentration. Modelled diffusion profile (*right*) for different elapsed times (*grey lines*) compared with element gradient (*black line*). Ti content normalized across transition marked by *dashed rectangle*. Time representing best fit is coded by a *solid grey line*, and *dashed grey line* is for comparison. *Inset* shows the results of 1D analytical diffusion method that accounts for the angle (α) between the measured profile and the perpendicular to the boundary of interest

a growth rate of >1–4 μm year^{-1} (3×10^{-7} to 12×10^{-7} μm s^{-1}). Crystal fragments show no overgrowths or diffusion profiles at fractured margins (Fig. 3), implying they had insufficient time to respond to changing PT conditions and indicating quenching on eruption. The lack of a prolonged diffusive re-equilibration history is, however, suggestive of geologically rapid accumulation of the melt-dominant magma body in its final stages prior to eruption (cf. Wilson and Charlier 2009; Brown and Fletcher 1999). These short time intervals suggest that the thermal/pressure/compositional perturbation may represent a mechanism that contributed to the final evacuation of the chamber.

Diffusion timescale results compare well with those presented by Saunders et al. (2010) where Whakamaru quartz core–rim boundaries yield times of 46–172 year, with a peak likelihood of renewed quartz growth at 50–70 year. Our timescales are also similar to the quartz records from Bishop Tuff and Campanian Ignimbrite, which also display Ti concentration changes considered

equivalent to 100°C heating over periods of probably no more than ~100 year before eruption (Wark et al. 2007; Pappalardo et al. 2008). In contrast, Oruanui quartz shows a great variety of CL zonation patterns (Liu et al. 2006), despite clear evidence for pre- and syn-eruptive mafic recharge (Wilson et al. 2006).

Heat flow associated with mafic recharge

We infer that the prominent change in Ti composition in quartz was associated with an injection of mafic magma, as this is known to play a significant role in the behaviour of shallow silicic melt-dominant chambers in the TVZ (e.g., Leonard et al. 2002; Wilson et al. 2006; Shane et al. 2007, 2008b). In addition, some Rangitaiki pumices display mingled textures, with the dominant silicic melt co-existing with hornblende-bearing juvenile mafic material (Table 1; Supplementary Data 3), showing that the silicic and mafic magmas were in contact during eruption. The preservation of these mingled textures in the Rangitaiki pumice and the lack of an intermediate mixed composition are consistent with a sudden injection of mafic magma immediately prior to, and possibly triggering, eruption. The observed mafic mixing in Rangitaiki pumices is clearly a syn-eruptive phenomenon, however, and a different event to the recharge event that most likely influenced the earlier growth of bright-CL quartz crystal rims.

An energy conservation model was used to test the feasibility of raising the magma reservoir temperature by ~100°C and causing the observed crystal resorption through mafic underplating. Our modelling assumed that the change in quartz rim compositions is solely due to temperature rise (with constant melt composition, pressure and a_{TiO_2}); that the mafic input magma was basaltic (using the average composition of mixed basaltic Whakamaru pumices, Supplementary Data 3) and added in a single pulse; and that it lost heat convectively to the rhyolitic chamber while it cooled and crystallized. Parameters used in calculations are summarized in Table 4.

Table 4 List of parameters and symbols used in thermodynamic calculations

Thermodynamic parameter	Symbol	Value	Units	References
Initial melt fraction in the mush (locking point)	φ_{ini}	0.5		
Change in crystallinity in mush	φ	0.15		
Specific heat of intrusion	Cp	1,500	J kg^{-1} K^{-1}	–[a]
Specific heat of mush	Cp	1,300	J kg^{-1} K^{-1}	–[a,b,c]
Density intrusion	ρ_i	2,900	kg m^{-3}	–[a,d]
Density mush	ρ_m	2,400	kg m^{-3}	–[a,e,f]
Latent heat of intrusion	L	4.00E+05	J kg^{-1} K^{-1}	–[c]
Latent heat of mush	L	2.70E+05	J kg^{-1} K^{-1}	–[a]
Intrusion emplacement temperature	T_{int}	900–1,100	°C	
Eruption temperature (final T intrusion, mush)	T_{fin}	770	°C	
Difference in density that drives convection	$\Delta\rho$	10–100	kg m^{-3}	
Thermal diffusivity	K	10^{-6}	m^2 s^{-1}	
Viscosity	μ	10^5	Pa s	–[b,d,g]
Chamber volume	V	1,000	km^3	–[h]
Chamber (mush) thickness (vol/surface area)	H	1	km	
Intrusion thickness	H_i	1	km	
Magma chamber depth	D	5	km	
Acceleration due to gravity	g	9.81	m^2s^{-1}	
Ideal gas constant	R	8.314	J K^{-1} mol^{-1}	
Thermal conductivity of host rocks	k	2	W m^{-1} K^{-1}	

[a] Wark et al. (2007)

[b] Bachmann and Bergantz (2006)

[c] Michaut and Jaupart (2010)

[d] Cottrell et al. (1999)

[e] Tait et al. (1989)

[f] Blake and Ivey (1986)

[g] Scaillet et al. (1998)

[h] Brown et al. (1998)

MELTS (Ghiorso and Sack 1995; Asimow and Ghiorso 1998; Gualda et al. 2010) was used to calculate the increase in crystallinity of the mafic intrusion during cooling, at 200 MPa and 3–4 wt% H_2O. Variation in crystallinity with temperature for mafic magma can be described by

$$\text{Crystallinity}_{\text{int}} = 0.441\text{erfc}(7.9 \times 10^{-3} \times T - 7.55), \quad (13)$$

where $\text{crystallinity}_{\text{int}}$ is the intrusion crystal content and T is temperature, °C (Fig. 9a). The change in melt fraction in the rhyolitic reservoir between emplacement and eruption temperatures is estimated as 0.15, implying a reduction in crystallinity from 50% to 35%. This assumes an initial (locked) crystal mush, with the crystal-rich (30–40%) *Type A* pumice representing the final magma crystallinity. Enthalpy loss (ΔE_i) by the intrusion

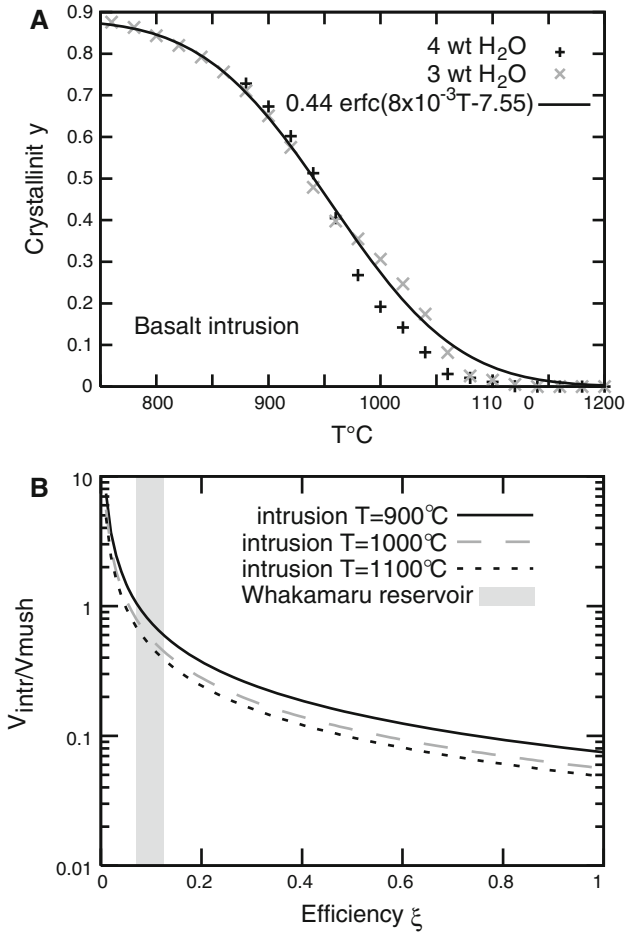

Fig. 9 Thermodynamic considerations for the underplating mafic intrusion. **a**—Basalt crystallinity decreases with increasing temperature. *Curves* derived from MELTS (Ghiorso and Sack 1995) using an average basaltic Whakamaru pumice composition; solid line represents a least-square fit for basaltic magma of 4 wt% H_2O; **b**—Volume ratio of magma (intrusion/mush) as a function of melting efficiencies; *grey shaded* region highlights the most probably range of efficiencies (from Dufek and Bergantz 2005)

$$\Delta E_{\text{i}} = V_{\text{i}} \left[\int_{T_{\text{i,ini}}}^{T_{\text{e}}} \rho_i c_i \text{d}T + \int_{\phi_{\text{i,ini}}}^{\phi_{\text{i}f}} \rho_{\text{i}} L_{\text{i}} d\phi \right], \quad (14)$$

can be related to enthalpy change in the mush

$$\Delta E_{\text{m}} = V_{\text{m}} \left[\int_{T_{\text{m,ini}}}^{T_{\text{e}}} \rho_{\text{m}} c_{\text{m}} \text{d}T + \int_{\phi_{\text{m,ini}}}^{\phi_{\text{m}f}} \rho_{\text{m}} L_{\text{m}} d\phi \right], \quad (15)$$

assuming an efficiency ξ (fraction of excess enthalpy of intrusion transferred to the mush, from Huber et al. 2010a, b) where

$$\xi \Delta E_{\text{i}} = \Delta E_{\text{m}}. \quad (16)$$

Here, subscripts i and m refer to intrusion and mush; T_{ini}, f_{ini} and T_{e} are, respectively, the temperature and melt fraction of the magma at the time of intrusion emplacement and eruption temperature (see also Table 4).

Intrusion efficiency is calculated using the fit of Fig. 9a, with results illustrated in Fig. 9b showing the intrusion/mush volume ratio as a function of melting efficiency. In a completely efficient process, all enthalpy associated with cooling and crystallizing intruded magma would heat and melt only the magma reservoir below which it ponds (Dufek and Bergantz 2005). The most likely range of efficiencies is, however, ~5–10%, where the intrusions are vertically stacked and cool on both sides (Dufek and Bergantz 2005; Fig. 9b), suggesting a 1:1 intrusion/mush ratio. We thus estimate that ~1,000 km^3 of basaltic magma would be required to heat the 1,000 km^3 rhyolite magma reservoir by 100°C, resulting in crystal dissolution followed by high-temperature rim crystallization. We estimate also that the chamber and underlying intrusion are ~1 km thick (mush thickness = volume/surface area).

There are several difficulties with this model of rapid or incremental injection of large volumes of mafic magma, however. Physical constraints with respect to the required accommodation space and efficiency of heat transfer through a thick cumulate pile are problematic. Furthermore, interaction between the underlying basaltic intrusion and rhyolitic chamber is likely to have been minimal due to the density differences. An additional energy source is required if we are to invoke thermal reactivation of the mush by mafic magma injection alone. Huber et al. (2011) suggest that internal overpressurization of the mush induced by small amounts of melting (10–20%) can break the crystalline framework by microfracturing, allowing for more efficient unlocking and accelerating self-assimilation of the chamber and surrounding crustal lithologies. The volume of mafic underplating magma required in our heat balance model could be significantly reduced by this—to values requiring more feasible accommodation space. It is also possible that although the change in

volume may be responsible for unlocking the mush, the critical factor in the reactivation process is the thermal budget.

Although our calculations indicate the involvement of a substantial volume of mafic magma, physical constraints mean that most of this mafic magma was not erupted, but instead provided the thermal feedback necessary to trigger processes in the silicic reservoir above. The 'gas sparging' model of Bachman and Bergantz (2006) may also apply here, whereby the underplating mafic magmas transport heat to the overlying crystal-rich rhyolitic chamber through the upward migration of a hot volatile phase. With volatile fluxes of >0.1 m^3 m^{-2} $year^{-1}$, a large reservoir would require a significant volume of volatiles, however, which would require multiple sparging episodes to rejuvenate the crystal mush, taking up to 100–200 ka (Bachmann and Bergantz 2006). It is clear, however, that generation and differentiation of the silicic magma must have taken a significant period of time, of which the quartz records only the final reheating stage prior to eruption.

Driving mechanisms for quartz zoning patterns: magma chamber models

A significant change in late-stage growth conditions clearly affected a majority of the observed quartz crystals. We assumed above that temperature is the dominant control on Ti concentration in quartz, although we cannot discount or measure the effects of changes in pressure and melt composition. As there is an abrupt change in composition within the Whakamaru quartz crystals, it is clearly not associated with gradual movements of crystals within the system as proposed for Bishop Tuff (Wallace et al. 1999; Anderson et al. 2000).

Two end-member scenarios are therefore proposed below (Fig. 10) to explain the distinct quartz zoning: (1) abrupt temperature increase and (2) significant pressure change, with both scenarios involving concomitant compositional changes affecting melt a_{TiO_2}. These scenarios invoke an episode (or episodes) of mafic recharge that provides the driving force for subsequent temperature, pressure or composition changes.

Temperature changes

Mafic melts play an important role in the generation of large silicic magma bodies (e.g., Hildreth 1981, 2004; Folch and Marti 1998; Annen et al. 2006). Models suggest that hot, volatile-rich melts enter the upper crust and induce melting of the crust and any plutonic bodies within it, generating the silicic melt (e.g., Bachmann and Bergantz 2006; Wark et al. 2007), in addition to the fundamental role of fractional crystallization of mafic parents in generating silicic melts. In the lifetime of any large silicic magma body, there are likely to have been innumerable recharge events that contributed heat and material to the system. Whakamaru quartz crystals appear to record the most significant of these, as well as minor temperature oscillations which shifted conditions out of the quartz stability field, resulting in dissolution.

The bimodal quartz Ti distributions observed here, and the temperature profiles at fixed pressure (Fig. 4), indicate that there were two phases of crystal growth: initially under low-temperature and then high-temperature conditions (assuming constant melt composition and a_{TiO_2}). The high-Ti overgrowth boundaries on CL-zoned quartz crystals typically truncate growth zoning within the core and hence represent changes associated with a recharge event which would also cause the observed partial dissolution prior to high-temperature rim growth. Our model (Fig. 10) thus invokes initial lower-temperature crystallization followed by a significant recharge event during which hot mafic magma is injected into the deeper parts of the magma system (as for Bishop Tuff; Hildreth 1979; Anderson et al. 2000; Wark et al. 2007). This thermal pulse results in an initial resorption of crystals as quartz becomes unstable, after which rims crystallize at higher temperature if (a) the pressure drops or (b) the injected mafic magma is CO_2 rich, which would decrease XH_2O (although if magma is close to water saturation, this will only have a minor effect), raise the solidus temperature and affect a_{TiO_2} (Wark et al. 2007).

The detailed growth zonation preserved within bright-CL crystal rims (Fig. 4) indicates that there may have been multiple minor recharge pulses during crystallization of the high-temperature rims. This complex oscillatory zoning may also have been due to fluctuations in a_{TiO_2}, small temperature variations, textural instability at the growing crystal front within the melt (Allegre et al. 1981) or competing diffusion and crystal growth rate.

Pressure changes

Although the Ti/pressure relationships proposed by Thomas et al. (2010) yield unrealistic absolute pressures for Whakamaru quartz crystallization, there remains the possibility that pressure affects Ti concentrations in quartz. Assuming uniform temperature and composition, dark-CL quartz cores would imply crystallization at higher pressures, followed by lower-pressure crystallization of bright-CL rims. The truncated core CL zones could reflect resorption during adiabatic ascent of the magma and its crystal cargo, with ponding and re-equilibration at shallower levels where bright-CL rims crystallized (Thomas et al. 2010). Mafic recharge could be the mechanism triggering magma ascent, by lowering magma density in response to an influx of volatiles or temperature increase (e.g., Folch and Marti 1998; Snyder 2000). However, it is difficult to envisage temperatures and melt compositions remaining uniform under such circumstances.

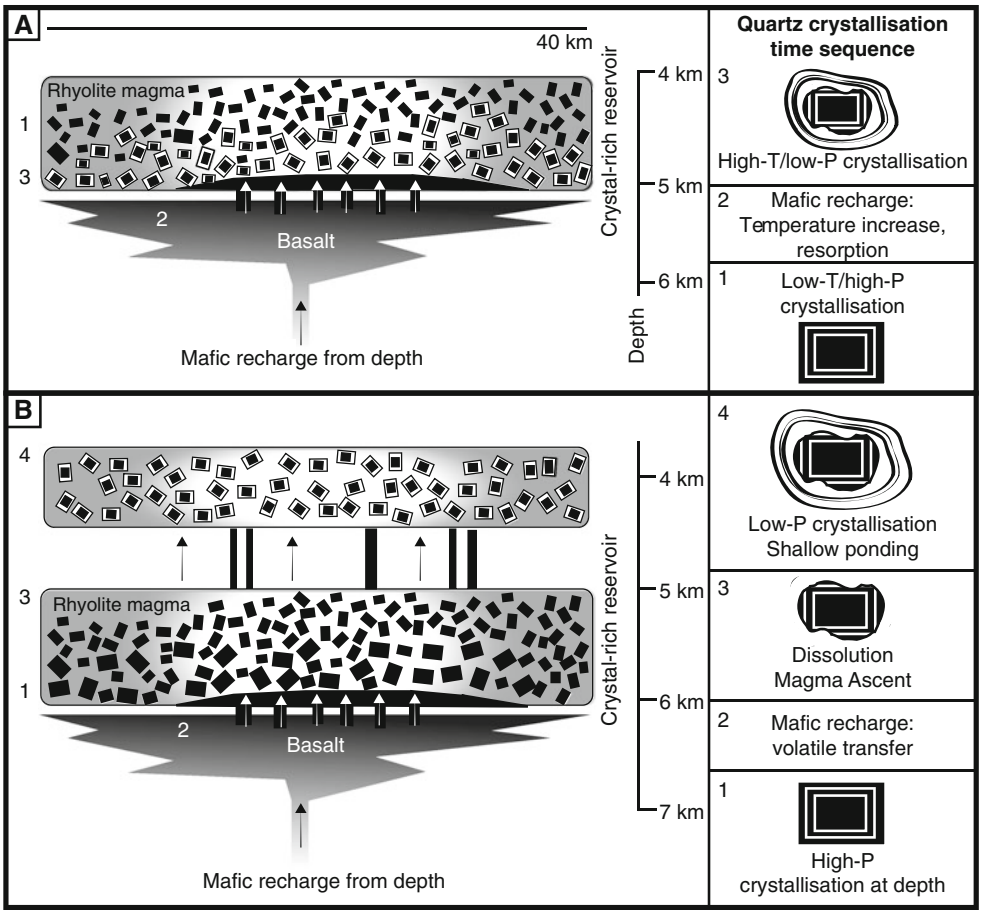

Fig. 10 Model for magma chamber processes responsible for the generation of quartz crystal zonation patterns. Magma reservoir holds Whakamaru magma of Type *A* composition, according to the Brown et al. (1998) classification. *Note*: depth scale for magma reservoirs is based on data from quartz melt-inclusion volatiles from Liu et al. (2006) and glass compositions; *horizontal scale* is derived from the estimates of the caldera width from field geology. **a**—Single magma chamber model—Time 1 represents crystallization at low temperature/high pressure within a crystal mush at depth; Time 2: Basaltic magma ponds at depth beneath the voluminous rhyolitic crystal mush, causing a temperature increase and resulting in resorption of quartz; Time 3: High-Ti (high-temperature or low-pressure) crystallization of quartz rims prior to eruption. High-Ti quartz crystallization could also be attributed here to a pressure drop associated with a smaller precursor eruption or partial degassing. **b**—Two-stage magma ponding—Time 1 represents crystallization of high-pressure quartz cores at depth, with some minor fluctuations (in T/P or a_{TiO_2}) producing subtle oscillatory zonation; Time 2: mafic recharge and ponding of mafic magma at base of rhyolitic mush causes a pressure change; Time 3: rhyolitic magma ascent accompanied by dissolution/resorption of quartz crystals; Time 4: Low-pressure rims crystallize during ponding and re-equilibration at shallow depths prior to eruption

Drawing on these considerations, we consider a mechanism by which low-Ti followed by high-Ti quartz could be crystallized in a single magma chamber (Fig. 10a). Initial low-Ti quartz crystallization would occur at depth within the large crystal-rich magma reservoir. Then, in order for the high-Ti, low-pressure quartz rims to crystallize, we must invoke either (a) a small eruption prior to the main caldera-forming event (for which there is no direct evidence) or (b) changes in volatile species in response to mafic magma interaction (altering the H_2O–CO_2 balance).

The zones could reflect two-stage evolution of the magma body (Fig. 10b), as for the Minoan rhyodacite (Cottrell et al. 1999) and the Bandelier magmatic system (Campbell et al. 2009), and the two-stage rhyolite magma-storage Rotorua eruption model (Smith et al. 2004). Our model involves the crystallization of dark-cored quartz (and other crystal phases) at depth followed by injection of mafic magma to underplate the rhyolitic crystal mush and provide enough thermal energy to resorb the quartz crystals and initiate magma chamber stirring (e.g., Huber et al. 2009). The reactivated mush then rises to shallower depths where quartz re-equilibrates and crystallizes lower-pressure, higher-temperature rims prior to eruption. The pressures and depths suggested by the Thomas et al. (2010) model cannot be satisfactorily applied in a TVZ context, as crystallization in the upper mantle is implied. We therefore assume magma reservoir depths derived from pressure estimates pertaining to quartz melt-inclusion volatile contents (Liu et al. 2006) and amphibole and glass chemistry, all of which suggest magma storage at <6 km.

There are some complications associated with this two-stage magma-ponding model. First, the reactivated magma which ponds at shallow crustal levels must still be crystal rich and of high viscosity, which is difficult to explain in terms of a crystal mush model. Secondly, the thickness of the crust in central TVZ (6–7 km; Bryan et al. 1999) means that there are limitations in terms of the thickness of a magma chamber pile which can be accommodated within the crust. In addition, if we consider that the timescale for quartz residence in the upper reservoir is <100 year, this would imply that the transfer of 1,000 km^3 of crystal-rich, extremely viscous magma occured in a shorter timescale from a deeper reservoir to the shallow one. This is a significant mass of magma to be transferred, and it would require additional energy sources to account for this phase of magma transport. Given these limitations of a model whereby pressure changes are the main driving force of quartz zonation, the temperature-controlled scenario (Fig. 10a) is preferred for the Whakamaru magma systems.

Conclusions

Complex zoning is observed in the volumetrically important quartz crystals in Whakamaru eruption deposits. Crystals are characterized by cycles of resorption, accompanied by temperature/pressure/compositional fluctuations, as recorded in the CL zonation and Ti concentration profiles. These variations in crystal zoning cannot be generated solely through closed-system process (e.g., crystallization) and thus indicate that the systems were open to recharge. It is particularly noted that overgrowths encase truncated CL growth zoning within the dark cores, indicating a major period of resorption, heating and subsequent re-growth, consistent with recharge and multistage crystallization. The major step in Ti content (and CL brightness) towards the crystal rims provides evidence for a magma chamber recharge event resulting in the elevation of temperature and/or a reduction in pressure and/or a change in melt chemistry, due to ponding at shallow crustal levels, and can be modelled as rapid rejuvenation of a crystal mush to a melt-dominant body.

Two 'conventional' end-member mechanisms for the formation of high-Ti quartz rims are (1) a thermal pulse due to mafic underplating of the rhyolitic crystal mush (e.g., Wark et al. 2007) or (2) adiabatic ascent of the magma resulting in a pressure reduction, resorption and crystallization of lower-pressure rims during shallow ponding (e.g., Thomas et al. 2010). The presence of mixed basaltic pumices in the Whakamaru and Rangitaiki ignimbrites provides evidence for syn-eruptive mafic recharge and mixing as a driving force during the eruption, and we infer that a similar event or events contributed to the resorption and Ti concentration variations recorded in the quartz.

Steep compositional gradients across the core–rim resorption horizon (<30 μm wide) preserved in all Whakamaru quartz crystals examined indicate maximum diffusion-controlled periods of 10–85 years for the last phase of crystallization prior to eruption. The lack of prolonged diffusion in the crystals (and thus preservation of complex internal zoning) is suggestive of short magma residence times following the significant thermal/pressure perturbation event. Thermodynamic calculations indicate that ~1,000 km^3 of mafic injection would be required to generate the 100°C thermal pulse recorded by the quartz (assuming that the Ti changes are due solely to temperature and that the whole of the Whakamaru magma body is represented by the sample suite). The Whakamaru magma reservoir system thus experienced a significant heating/decompression event shortly before catastrophic eruption, and its evolution over the time span represented by quartz crystals is punctuated by thermal events and/or ponding at different depths with re-equilibration prior to eruption.

Acknowledgments We thank Norman Charnley (University of Oxford) for his assistance with the electron microprobe work and helping acquire Ti-in-quartz data. Stuart Kearns (University of Bristol) is also acknowledged for his help with the CL imaging. We also thank Stephen Reed (University of Cambridge) for his interest in the CL of quartz during the early stages of this investigation. NEM acknowledges postgraduate funding from the Woolf Fisher Trust (New Zealand), and CJNW acknowledges support from the Marsden Fund (VUW0813) administered by the Royal Society of New Zealand. We thank Fidel Costa, an anonymous reviewer, journal editor Jon Blundy and Aidan Allan for their valuable comments.

Appendix

The derivation for the 1D analytical method is described in Fig. 11. This method provides a means of accounting for the angle between the diffusion transect and the line perpendicular to the core–rim boundary.

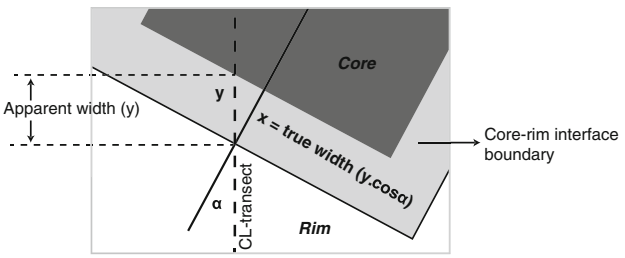

Fig. 11 Detail of the core–rim interface (*plan view*), where the *black dashed line* indicates the calibrated CL transect and the *black line* represents the ideal diffusion modelling profile, oriented perpendicular to the core–rim interface. In order to correct for this angle to the diffusion boundary, we consider the 'true' and 'apparent' widths of the transition zone, where the ratio of true/apparent widths is given by $x/y = y\text{Cos}\alpha/y = \cos\alpha$ (where α is the angle to perpendicular from the core–rim boundary)

References

Allegre CJ, Provost A, Jaupart C (1981) Oscillatory zoning: a pathological case of crystal growth. Nature 294:223–228

Anderson AT, Davis AM, Lu F (2000) Evolution of Bishop Tuff rhyolitic magma based on melt and magnetite inclusions and zoned phenocrysts. J Petrol 41:449–473

Annen C, Blundy J, Sparks RSJ (2006) The genesis of intermediate and silicic magmas in deep crustal hot zones. J Petrol 47:505–539

Asimow PD, Ghiorso MS (1998) Algorithmic modifications extending MELTS to calculate subsolidus phase relations. Am Mineral 83:1127–1131

Bachmann O, Bergantz GW (2006) Gas percolation in upper-crustal silicic crystal mushes as a mechanism for upward heat advection and rejuvenation of near-solidus magma bodies. J Volcanol Geotherm Res 149:85–102

Bacon CR, Hirschmann MM (1988) Mg/Mn partitioning as a test for equilibrium between coexisting Fe-Ti oxides. Am Mineral 73:57–61

Bibby HM, Caldwell TG, Davey FJ, Webb TH (1995) Geophysical evidence on the structure of the Taupo Volcanic Zone and its hydrothermal circulation. J Volcanol Geotherm Res 68:29–58

Bindeman I (2005) Fragmentation phenomena in populations of magmatic crystals. Am Mineral 90:1801–1815

Blake S, Ivey GN (1986) Magma-mixing and the dynamics of withdrawal from stratified reservoirs. J Volcanol Geotherm Res 27:153–178

Blake S, Wilson CJN, Smith IEM, Walker GPL (1992) Petrology and dynamics of the Waimihia mixed magma eruption, Taupo Volcano, New Zealand. J Geol Soc 149:193–207

Blundy J, Cashman K (2001) Ascent-driven crystallization of dacite magmas at Mount St Helens, 1980–1986. Contrib Mineral Petrol 140:631–650

Briggs ND (1976) Recognition and correlation of subdivisions within the Whakamaru Ignimbrite, central North Island, New Zealand. NZ J Geol Geophys 19:463–501

Brown SJA, Fletcher IR (1999) SHRIMP U-Pb dating of the preeruption growth history of zircons from the 340 ka Whakamaru Ignimbrite, New Zealand: Evidence for >250 k.y. magma residence times. Geology 27:1035–1038

Brown SJA, Wilson CJN, Cole JW, Wooden J (1998) The Whakamaru group ignimbrites, Taupo Volcanic Zone, New Zealand: evidence for reverse tapping of a zoned silicic magmatic system. J Volcanol Geotherm Res 84:1–37

Bryan CJ, Sherburn S, Bibby HM, Bannister S, Hurst AW (1999) Shallow seismicity of the central Taupo Volcanic Zone, New Zealand: its distribution and nature. NZ J Geol Geophys 42:533–542

Campbell ME, Hanson JB, Minarik WG, Stix J (2009) Thermal history of the Bandelier magmatic system: evidence for magmatic injection and recharge at 1.61 Ma as revealed by cathodoluminescence and titanium geothermometry. J Geol 117:469–485

Charlier BLA, Wilson CJN, Davidson JP (2008) Rapid open-system assembly of a large silicic magma body: time-resolved evidence from cored plagioclase crystals in the Oruanui eruption deposits, New Zealand. Contrib Mineral Petrol 156:799–813

Charlier BLA, Wilson CJN, Mortimer N (2010) Evidence from zircon U-Pb age spectra for crustal structure and felsic magma genesis at Taupo volcano, New Zealand. Geology 38:915–918

Cherniak DJ, Watson EB, Wark DA (2007) Ti diffusion in quartz. Chem Geol 236:65–74

Cole JW (1990) Structural control and origin of volcanism in the Taupo Volcanic Zone, New Zealand. Bull Volcanol 52:445–459

Costa F, Morgan D (2011) Time constraints from chemical equilibration in magmatic crystals. In: Dosseto A, Turner SP, Van Orman JA (eds) Timescales of magmatic processes: from core to atmosphere. Wiley, Chichester, pp 125–159

Costa F, Dohmen R, Chakraborty S (2008) Time scales of magmatic processes from modeling the zoning patterns of crystals. Rev Mineral Geochem 69:545–594

Cottrell E, Gardner JE, Rutherford MJ (1999) Petrologic and experimental evidence for the movement and heating of the pre-eruptive Minoan rhyodacite (Santorini, Greece). Contrib Mineral Petrol 135:315–331

Devine JD, Rutherford MJ, Norton GE, Young SR (2003) Magma storage region processes inferred from geochemistry of Fe-Ti oxides in andesitic magma, Soufriere Hills volcano, Montserrat, W.I. J Petrol 44:1375–1400

Dufek J, Bergantz GW (2005) Lower crustal magma genesis and preservation: a stochastic framework for the evaluation of basalt-crust interaction. J Petrol 46:2167–2195

Ewart A (1965) Mineralogy and petrogenesis of the Whakamaru Ignimbrite in the Maraetai area of the Taupo Volcanic Zone, New Zealand. NZ J Geol Geophys 8:611–677

Folch A, Marti J (1998) The generation of overpressure in felsic magma chambers by replenishment. Earth Planet Sci Lett 163:301–314

Froggatt PC, Nelson CS, Carter L, Griggs G, Black KP (1986) An exceptionally large late quaternary eruption from New Zealand. Nature 319:578–582

Ghiorso MS, Evans BW (2008) Thermodynamics of rhombohedral oxide solid solutions and a revision of the Fe-Ti two-oxide geothermometer and oxygen-barometer. Am J Sci 308:957–1039

Ghiorso MS, Sack RO (1995) Chemical mass transfer in magmatic processes. IV. A revised and internally consistent thermodynamic model for the interpolation and extrapolation of liquid-solid equilibria in magmatic systems at elevated temperatures and pressures. Contrib Min Pet 119:197–212

Götze J, Plötze M, Habermann D (2001) Origin, spectral characteristics and practical applications of the cathodoluminescence (CL) of quartz—a review. Mineral Petrol 71:225–250

Götze J, Plötze M, Graupner T, Hallbauer DK, Bray CJ (2004) Trace element incorporation into quartz: a combined study by ICP-MS, electron spin resonance, cathodoluminescence, capillary ion analysis, and gas chromatography. Geochim Cosmochim Acta 68:3741–3759

Graham IJ, Cole JW, Briggs RM, Gamble JA, Smith IEM (1995) Petrology and petrogenesis of volcanic rocks from the Taupo Volcanic Zone: a review. J Volcanol Geotherm Res 68:59–87

Gualda GAR, Ghiorso MS, Vaum R, Carley TL (2010) Rhyolite-MELTS: a modified calibration of MELTS optimized for silica-rich, fluid-bearing magmatic systems. American Geophysical Union, Fall meeting 2010, abstract V43A-2352

Hammer JE (2008) Experimental studies of the kinetics and energetic of magma crystallization. Rev Mineral Geochem 69:9–59

Hammer JE, Rutherford MJ (2002) An experimental study of the kinetics of decompression-induced crystallization in silicic melt. J Geophys Res 107(B1):2021. doi:10.1029/2001JB000281

Harrison AJ, White RS (2004) Crustal structure of the Taupo Volcanic Zone, New Zealand: stretching and igneous intrusion. Geophys Res Lett 31:L13615. doi:10.1029/2004GL019885

Hayden LA, Watson EB (2007) Rutile saturation in hydrous siliceous melts and its bearing on Ti-thermometry of quartz and zircon. Earth Planet Sci Lett 258:561–568

Hayden LA, Watson EB, Wark DA (2005) Rutile saturation and TiO_2 diffusion in hydrous siliceous melts. EOS Trans Am Geophys Un 86 (52, Fall meeting Suppl): MR13A-0076

Hildreth W (1979) The Bishop Tuff: evidence for the origin of compositional zonation in silicic magma chambers. In: Chapin CE, Elston WE (eds) Ash-flow tuffs. Geol Soc of America, Spec paper 180, pp 43–75

Hildreth W (1981) Gradients in silicic magma chambers: implications for lithospheric magmatism. J Geophys Res 86:10153–10192

Hildreth W (2004) Volcanological perspectives on Long Valley, Mammoth Mountain, and Mono Craters: several contiguous but discrete systems. J Volcanol Geotherm Res 136:169–198

Hochstein MP (1995) Crustal heat transfer in the Taupo Volcanic Zone (New Zealand): comparison with other volcanic arcs and explanatory heat source models. J Volcanol Geotherm Res 68:117–151

Holland TJB, Powell R (1998) An internally-consistent dataset for phases of petrological interest. J Metam Petrol 16:309–344

Huber C, Bachmann O, Manga M (2009) Homogenization processes in silicic magma chambers by stirring and mushification (latent heat buffering). Earth Planet Sci Lett 283:38–47

Huber C, Bachmann O, Dufek J (2010a) The limitations of melting on the reactivation of silicic mushes. J Volcanol Geotherm Res 195:97–105

Huber C, Bachmann O, Manga M (2010b) Two competing effects of volatiles on heat transfer in crystal-rich magmas: thermal insulation vs. defrosting. J Petrol 51:847–867

Huber C, Bachmann O, Dufek J (2011) Thermo-mechanical reactivation of locked crystal mushes: melting-induced internal fracturation and assimilation processes in magmas. Earth Planet Sci Lett 304:443–454

Huebner JS, Sato M (1970) The oxygen fugacity-temperature relationships of manganese oxide and nickel oxide buffers. Am Mineral 55:934–952

Humphreys MCS, Blundy JD, Sparks RSJ (2006) Magma evolution and open-system processes at Shiveluch volcano: insights from phenocryst zoning. J Petrol 47:2303–2334

Leonard GS, Cole JW, Nairn IA, Self S (2002) Basalt triggering of the c. AD 1305 Kaharoa rhyolite eruption, Tarawera Volcanic Complex, New Zealand. J Volcanol Geotherm Res 115:461–486

Linden PF, Redondo JM (1991) Molecular mixing in Rayleigh-Taylor instability. Part I: global mixing. Phys Fluids A 3:1269–1277

Liu Y, Anderson AT, Wilson CJN, Davis AM, Steele IM (2006) Mixing and differentiation in the Oruanui rhyolitic magma, Taupo, New Zealand: evidence from volatiles and trace elements in melt inclusions. Contrib Mineral Petrol 151:71–87

Martin RC (1965) Lithology and eruptive history of the Whakamaru Ignimbrites in the Maraetai area of the Taupo Volcanic Zone, New Zealand. NZ J Geol Geophys 8:680–701

Martin VM, Morgan DJ, Jerram DA, Caddick MJ, Prior DJ, Davidson JP (2008) Bang! Month-scale eruption triggering at Santorini Volcano. Science 321:1178

McCulloch MT, Kyser TK, Woodhead JD, Kinsey L (1994) Pb-Sr-Nd-O isotopic constraints on the origin of rhyolites from the Taupo Volcanic Zone of New Zealand: evidence for assimilation followed by fractionation from basalt. Contrib Mineral Petrol 115:303–312

Michaut C, Jaupart C (2010) Two models for the formation of magma reservoirs by small increments. Tectonophysics (in press). doi:10.1016/j.tecto.2009.08.019

Morgan DJ, Blake S, Rogers NWB, DeVivo B, Rolandi G, Macdonald R, Hawkesworth CJ (2004) Time scales of crystal residence and magma chamber volume from modelling of diffusion profiles in phenocrysts: Vesuvius 1944. Earth Planet Sci Lett 222:933–946

Nairn IA, Shane PR, Cole JW, Leonard GJ, Self S, Pearson N (2004) Rhyolite magma processes of the AD 1315 Kaharoa eruption episode, Tarawera volcano, New Zealand. J Volcanol Geotherm Res 131:265–294

Pappalardo L, Ottolini L, Mastrolorenzo G (2008) The Campanian Ignimbrite (southern Italy) geochemical zoning: insight on the generation of a super-eruption from catastrophic differentiation and fast withdrawal. Contrib Mineral Petrol 156:1–26

Peppard BT, Steele IM, Davis AM, Wallace PJ, Anderson AT (2001) Zoned quartz phenocrysts from the rhyolitic Bishop Tuff. Am Mineral 86:1034–1052

Pillans BJ, Kohn BP, Berger GW, Froggatt PC, Duller GAT, Alloway BV, Hesse PP (1996) Multi-method dating comparison for mid-Pleistocene Rangitawa Tephra, New Zealand. Quat Sci Rev 15:641–653

Putirka KD (2005) Igneous thermometers and barometers based on plagioclase + liquid equilibria: tests of some existing models and new calibrations. Am Mineral 90:336–346

Putirka KD (2008) Thermometers and Barometers for Volcanic Systems. In: Putirka K, Tepley F (eds) Minerals, inclusions and Volcanic processes, reviews in mineralogy and geochemistry, mineralogical, Soc Am 69, pp 61–120

Reid MR, Vazquez JA, Schmitt AK (2010) Zircon-scale insights into the history of a supervolcano, Bishop Tuff, Long Valley, California, with implications for the Ti-in-zircon geothermometer. Contrib Mineral Petrol (in press). doi:10.1007/s00410-010-0532-0

Ridolfi F, Renzulli A, Puerini M (2010) Stability and chemical equilibrium of amphibole in calc-alkaline magmas: an overview, new thermobarometric formulations and application to subduction-related volcanoes. Contrib Mineral Petrol 160:45–66

Ruprecht P, Bergantz GW, Dufek J (2008) Modeling of gas-driven magmatic overturn: tracking of phenocryst dispersal and gathering during magma mixing. Geochem Geophysics Geosyst 9(7):Q07017. doi:10.1029/2008GC002022

Rusk BG, Lowers HA, Reed MH (2008) Trace elements in hydrothermal quartz: relationships to cathodoluminescent textures and insights into vein formation. Geology 36:547–550

Saunders KE, Morgan DJ, Baker JA, Wysoczanski RJ (2010) The magmatic evolution of the Whakamaru supereruption, New Zealand, constrained by a microanalytical study of plagioclase and quartz. J Petrol 51:2465–2488

Scaillet B, Holtz F, Pichavant M (1998) Phase equilibrium constraints on the viscosity of silicic magmas 1. Volcanic-plutonic comparison. J Geophys Res 103:257–266

Shane P, Martin SB, Smith VC, Beggs KF, Darragh MB, Cole JW, Nairn IA (2007) Multiple rhyolite magmas and basalt injection in the 17.7 ka Rerewhakaaitu eruption episode from Tarawera volcanic complex, New Zealand. J Volcanol Geotherm Res 164:1–26

Shane P, Smith VC, Nairn IA (2008a) Millenial timescale resolution of rhyolite magma recharge at Tarawera volcano: insights from quartz chemistry and melt inclusions. Contrib Mineral Petrol 155:397–411

Shane P, Nairn IA, Smith VC, Darragh M, Beggs KF, Cole JW (2008b) Silicic recharge of multiple rhyolite magmas by basaltic intrusion during the 22.6 ka Okaraka eruption episode, New Zealand. Lithos 103:527–549

Shaw C (2004) The temporal evolution of three magmatic systems in the West Eifel volcanic field, Germany. J Volcanol Geotherm Res 131:213–240. doi:10.1016/S0377-0273(03)00363-9

Smith VC, Shane P, Nairn IA (2004) Reactivation of a rhyolitic magma body by a new rhyolitic intrusion before the 15.8 ka Rotorua eruptive episode: implications for magma storage in the Okataina Volcanic Centre, New Zealand. J Geol Soc Lond 161:757–772

Smith VC, Blundy JD, Arce JL (2009) A temporal record of magma accumulation and evolution beneath Nevado de Toluca, Mexico, preserved in plagioclase phenocrysts. J Petrol 50:405–426

Smith V, Shane P, Nairn I (2010) Insights into silicic melt generation using plagioclase, quartz and melt inclusions from the caldera-

forming Rotoiti eruption, Taupo Volcanic Zone, New Zealand. Contrib Mineral Petrol 160:951–971. doi:10.1007/s00410-010-0516-0

Snyder D (2000) Thermal effects of the intrusion of basaltic magma into a more silicic magma chamber and implications for eruption triggering. Earth Planet Sci Lett 175:257–273

Sparks RSJ, Sigurdsson H, Wilson L (1977) Magma mixing: a mechanism for triggering explosive eruptions. Nature 267:315–318

Stern TA (1987) Asymmetric back-arc spreading, heat flux and structure associated with the Central Volcanic Region of New Zealand. Earth Planet Sci Lett 85:265–276

Stern TA, Stratford WR, Salmon ML (2006) Subduction evolution and mantle dynamics at a continental margin: central North Island, New Zealand. Rev Geophys 44:RG4002 paper 2005 RG000171

Stratford WR, Stern TA (2004) Strong seismic reflections and melts in the mantle of a continental back-arc basin. Geophys Res Lett 31:L06622. doi:10.1029/2003GL019232

Tait S (1992) Selective preservation of melt inclusions in igneous phenocrysts. Am Mineral 77:146–155

Tait S, Worner G, van den Bogaard P, Schmincke H (1989) Cumulate nodules as evidence for convective fractionation in a phonolite magma chamber. J Volcanol Geotherm Res 37:21–37

Thomas JB, Watson EB, Spear FS, Shemella PT, Nayak SK, Lanzirotti A (2010) TitaniQ under pressure: the effect of pressure and temperature on the solubility of Ti in quartz. Contrib Mineral Petrol 160:743–759

Venezky DU, Rutherford MJ (1999) Petrology and Fe-Ti oxide reequilibration of the 1991 Mount Unzen mixed magma. J Volcanol Geotherm Res 89:213–230

Wallace PJ, Anderson AT, Davis AM (1999) Gradients in H_2O, CO_2, and exsolved gas in a large-volume silicic magma system: interpreting the record preserved in melt inclusions from the Bishop Tuff. J Geophys Res 104:20097–20122

Wark DA, Watson EB (2006) TitaniQ: a titanium-in-quartz geothermometer. Contrib Mineral Petrol 152:743–754

Wark DA, Hildreth W, Spear FS, Cherniak DJ, Watson EB (2007) Pre-eruption recharge of the Bishop magma system. Geology 35:235–238

Watt GR, Wright P, Galloway S, McLean C (1997) Cathodoluminescence and trace element zoning in quartz phenocrysts and xenocrysts. Geochim Cosmochim Acta 61:4337–4348

White RW, Powell R, Holland TJB, Worley BA (2000) The effect of TiO2 and Fe2O3 on metapelitic assemblages at greenschist and amphibolite facies conditions: mineral equilibria calculations in the system K2O-FeO-MgO-Al2O3-SiO2–H2O-TiO2-Fe2O3. J Metamorph Geol 18:497–511

White RW, Powell R, Clarke GL (2002) The interpretation of reaction textures in Fe-rich metapelitic granulites of the Musgrave Block, central Australia: constraints from mineral equilibria calculations in the system K2O-FeO-MgO-A2O3-SiO2–H2O-TiO2-Fe2O3. J Metamorph Geol 20:41–55

Wilson CJN, Charlier BLA (2009) Rapid rates of magma generation at contemporaneous magma systems, Taupo volcano, New Zealand: insights from U-Th model-age spectra in zircons. J Petrol 50:875–907

Wilson CJN, Houghton BF, Lloyd EF (1986) Volcanic history and evolution of the Maroa-Taupo area, central North Island. R Soc NZ Bull 23:194–223

Wilson CJN, Houghton BF, McWilliams MO, Lanphere MA, Weaver SD, Briggs RM (1995) Volcanic and structural evolution of Taupo Volcanic Zone, New Zealand: a review. J Volcanol Geotherm Res 68:1–28

Wilson CJN, Blake S, Charlier BLA, Sutton AN (2006) The 26.5 ka Oruanui eruption, Taupo volcano, New Zealand: development, characteristics and evacuation of a large rhyolitic magma body. J Petrol 47:35–69

Wilson CJN, Gravley DM, Leonard GS, Rowland JV (2009) Volcanism in the central Taupo Volcanic Zone, New Zealand: tempo, styles and controls. Spec Pub IAVCEI 2:225–247

Wilson CJN, Seward TM, Allan ASR, Charlier BLA, Bello L, Hildreth W (2011) Wilson CJN, Seward TM, Allan ASR, Charlier BLA, Bello L, Hildreth W (2011) A comment on: 'TitaniQ under pressure: the effect of pressure and temperature on the solubility of Ti in quartz' by Jay B. Thomas, E. Bruce Watson, Frank S. Spear, Philip T. Shemella, Saroj K. Nayak, and Antonio Lanzirotti. Contrib Mineral Petrol (submitted)